

# Elucidating CO<sub>2</sub> Chemisorption in Diamine-Appended Metal–Organic Frameworks

Alexander C. Forse,<sup>a,b,d</sup> Phillip J. Milner,<sup>a,e,†</sup> Jung-Hoon Lee,<sup>c,f</sup> Halle N. Redfearn,<sup>a</sup> Julia Oktawiec,<sup>a</sup> Rebecca L. Siegelman,<sup>a,e</sup> Jeffrey D. Martell,<sup>a</sup> Bhavish Dinakar,<sup>b,e</sup> Leo B. Porter-Zasada,<sup>a</sup> Miguel I. Gonzalez,<sup>a</sup> Jeffrey B. Neaton,<sup>\*c,f,g</sup> Jeffrey R. Long,<sup>\*a,b,e</sup> Jeffrey A. Reimer<sup>\*b,e</sup>

<sup>a</sup>Department of Chemistry, <sup>b</sup>Department of Chemical and Biomolecular Engineering, <sup>c</sup>Department of Physics, and <sup>d</sup>Berkeley Energy and Climate Institute, University of California, Berkeley, California 94720, U.S.A.

<sup>e</sup>Materials Sciences Division, Lawrence Berkeley National Laboratory, Berkeley, California 94720, U.S.A.

<sup>f</sup>Molecular Foundry, Lawrence Berkeley National Laboratory, Berkeley, California 94720, U.S.A.

<sup>g</sup>Kavli Energy Nanosciences Institute at Berkeley, Berkeley, California 94720, U.S.A.

**ABSTRACT:** The widespread deployment of carbon capture and sequestration as a climate change mitigation strategy could be facilitated by the development of more energy-efficient adsorbents. Diamine-appended metal–organic frameworks of the type diamine–M<sub>2</sub>(dobpdc) (M = Mg, Mn, Fe, Co, Ni, Zn; dobpdc<sup>4-</sup> = 4,4'-dioxidobiphenyl-3,3'-dicarboxylate) have shown promise for carbon capture applications, although questions remain regarding the molecular mechanisms of CO<sub>2</sub> uptake in these materials. Here, we leverage the crystallinity and tunability of this class of frameworks to perform a comprehensive study of CO<sub>2</sub> chemisorption. Using multinuclear nuclear magnetic resonance (NMR) spectroscopy experiments and van der Waals-corrected density functional theory (DFT) calculations for thirteen diamine–M<sub>2</sub>(dobpdc) variants, we demonstrate that the canonical CO<sub>2</sub> chemisorption products—ammonium carbamate chains and carbamic acid pairs—can be readily distinguished, and that ammonium carbamate chain formation dominates for diamine–Mg<sub>2</sub>(dobpdc) materials. In addition, we elucidate a new chemisorption mechanism in the material dmpn–Mg<sub>2</sub>(dobpdc) (dmpn = 2,2-dimethyl-1,3-diaminopropane), which involves formation of a 1:1 mixture of ammonium carbamate and carbamic acid and accounts for the unusual adsorption properties of this material. Finally, we show that the presence of water plays an important role in directing the mechanisms for CO<sub>2</sub> uptake in diamine–M<sub>2</sub>(dobpdc) materials. Overall, our combined NMR and DFT approach enables a thorough depiction and understanding of CO<sub>2</sub> adsorption within diamine–M<sub>2</sub>(dobpdc) compounds, which may aid similar studies in other amine-functionalized adsorbents in the future.

## INTRODUCTION

Carbon dioxide capture and sequestration at power stations and chemical manufacturing plants is anticipated to play an important role in efforts to mitigate greenhouse gas emissions.<sup>1</sup> Aqueous amine solutions are already used to capture CO<sub>2</sub> at some locations, including the recently retrofitted Petra Nova power station.<sup>2</sup> More energy efficient capture materials could accelerate the adoption of CO<sub>2</sub> capture as a mitigation strategy, and amine-functionalized adsorbents have emerged as promising next-generation materials that benefit from the highly selective chemistry of amines with CO<sub>2</sub>, similar to traditional amine solvents.<sup>3</sup> These materials may offer improvements over amine solutions including improved stability, reduced volatility, and lower regeneration temperatures.

Amine-appended metal–organic frameworks with the formula (diamine)<sub>2</sub>M<sub>2</sub>(dobpdc)—subsequently referred to here as diamine–M<sub>2</sub>(dobpdc)—in particular have shown exceptional promise for CO<sub>2</sub> capture<sup>4–13</sup> and are obtained by functionalizing the coordinatively-unsaturated metal sites in the M<sub>2</sub>(dobpdc) framework (M = Mg, Mn, Fe, Co, Ni, Zn; dobpdc<sup>4-</sup> = 4,4'-dioxidobiphenyl-3,3'-dicarboxylate) with diamines (Figure 1a,b).<sup>4,5,14–19</sup> Rather than displaying traditional Langmuir-type adsorption, many diamine–M<sub>2</sub>(dobpdc) materials exhibit step-shaped isotherms, corresponding to sudden adsorption of CO<sub>2</sub> upon exposure to a given thresh-

old pressure. This behavior arises as a result of an unprecedented cooperative adsorption mechanism whereby CO<sub>2</sub> inserts into each metal–amine bond to form ion-paired ammonium carbamate chains that propagate along the framework channels (down the crystallographic *c* axis, see Figure 1c).<sup>5,14,20</sup> Importantly, these materials exhibit high working capacities for CO<sub>2</sub> removal, and moreover relatively small changes in pressure and temperature can be used to trigger adsorption or desorption. Thus, these materials may afford substantial energy and cost savings when used in processes involving temperature or temperature-pressure swings.<sup>21–23</sup>

Recent single-crystal X-ray diffraction characterization of a series of diamine–Zn<sub>2</sub>(dobpdc) compounds revealed that the formation of ammonium carbamate chains occurs for a number of different diamines with diverse structures,<sup>14</sup> corroborating the results of other studies using powder X-ray diffraction.<sup>5,19</sup> The cooperative adsorption mechanism has been further validated at the atomic level using van der Waals-corrected density functional theory (vdW-corrected DFT) calculations,<sup>5,20,24,25</sup> which are able to predict binding enthalpies within a few kJ/mol of experiment. These binding enthalpies, in combination with a statistical mechanical model, have been used to explain the step-shaped isotherm in terms of an abrupt increase in the mean chain length at a critical CO<sub>2</sub> pressure.<sup>26</sup> Importantly, the adsorption thermodynamics—and therefore the step pressure at a given temperature—can be tuned by varying the met-

al<sup>15,15,20,27</sup> or the diamine,<sup>14–16,18</sup> allowing for the targeted design of materials for specific separations involving CO<sub>2</sub>. While single-crystal X-ray diffraction studies have been applied with great success to diamine-appended Zn<sub>2</sub>(dobpdc) variants,<sup>14,15,19</sup> the lack of large single crystals for the most technologically relevant magnesi-

um analogues, as well as the presence of structural disorder in some materials, necessitates the development of additional characterization methods to fully elucidate the factors dictating cooperative adsorption in this class of frameworks.

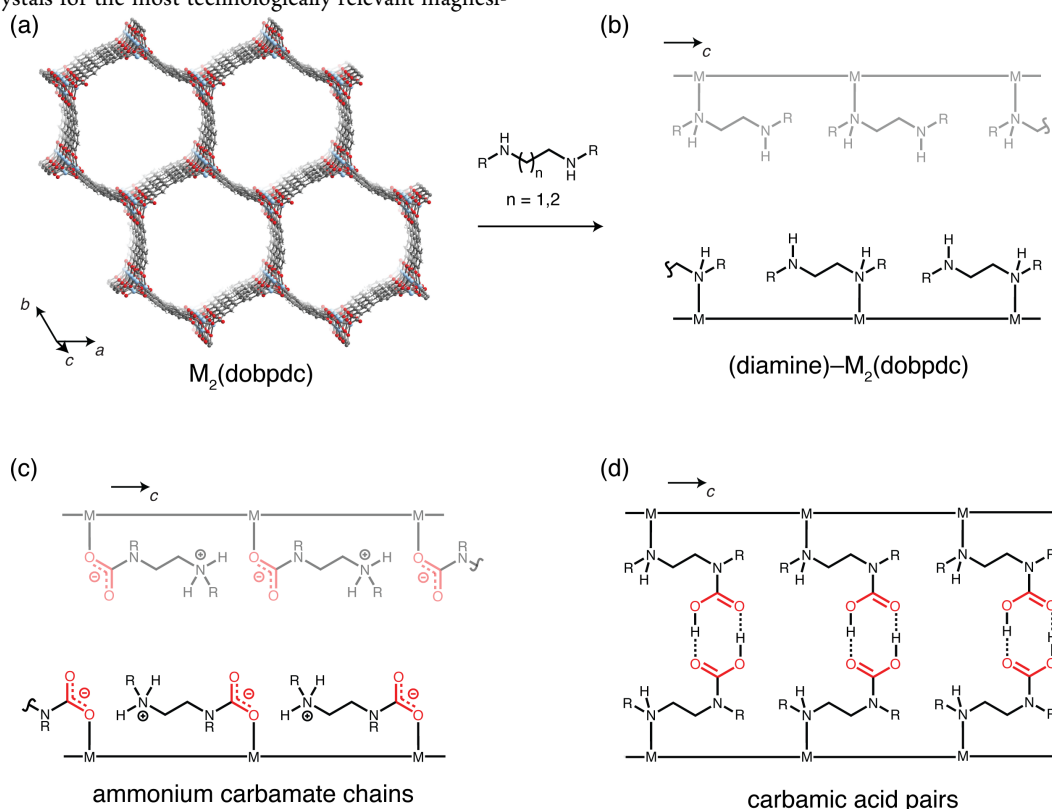


**Figure 1.** Canonical CO<sub>2</sub> chemisorption products in diamine-M<sub>2</sub>(dobpdc) materials. (a) Structure of the parent metal-organic framework, M<sub>2</sub>(dobpdc) (M = Mg, Mn, Fe, Co, Ni, Zn).<sup>28</sup> (b) Schematic structure of diamine-M<sub>2</sub>(dobpdc) materials, prepared by post-synthetic grafting of diamines to the open M<sup>2+</sup> sites of M<sub>2</sub>(dobpdc). (c) Ammonium carbamate chain formation upon CO<sub>2</sub> adsorption. (d) Carbamic acid pair formation upon CO<sub>2</sub> adsorption. Ammonium carbamate chains and carbamic acid pairs are the only chemisorption products that have been confirmed crystallographically to date in these materials.

We recently discovered that the material (dmpn)<sub>2</sub>Mg<sub>2</sub>(dobpdc) (dmpn = 2,2-dimethyl-1,3-diaminopropane) possesses an adsorption step in the optimum range for capture of CO<sub>2</sub> from coal flue gas, enabling a working capacity of 2.42 mmol/g (9.1 wt %) with a modest 60 °C temperature swing for adsorbent regeneration using pure CO<sub>2</sub>.<sup>15</sup> This material is also stable for at least 1000 adsorption-desorption cycles under humid conditions. Interestingly, gas adsorption, NMR, and X-ray diffraction measurements indicated that this material chemisorbs CO<sub>2</sub> by a mechanism that does not involve purely ammonium carbamate chain formation (Figure 1c). Indeed, NMR measurements showed that (dmpn)<sub>2</sub>Mg<sub>2</sub>(dobpdc) exhibits a *mixed* chemisorption mechanism that involves the formation of both ammonium carbamate and carbamic acid species.<sup>15</sup> Crystallographic and NMR studies of the isostructural (dmpn)<sub>2</sub>Zn<sub>2</sub>(dobpdc) analogue revealed that, rather than ammonium carbamate chains, carbamic acid pairs form at CO<sub>2</sub> gas pressures close to 1 bar,<sup>15</sup> a species that was first predicted computationally in this class of materials (Figure 1d).<sup>20,25,29</sup> At pressures below 1 bar, a mixed mechanism was again observed, with an unspecified arrangement of ammonium carbamate and carbamic acid groups.<sup>15</sup>

Here, we make use of the well-defined and readily modified structures of the diamine-M<sub>2</sub>(dobpdc) materials class to perform a

comprehensive study of CO<sub>2</sub> chemisorption using a combination of multinuclear NMR spectroscopy experiments and vdW-corrected DFT calculations. Many different diamine-appended variants can be synthesized and analyzed using this highly ordered system, making these materials invaluable for fundamental studies of CO<sub>2</sub> chemisorption. Furthermore, the techniques and spectroscopic signatures identified here may allow diamine-M<sub>2</sub>(dobpdc) frameworks to serve as a model system for the broader class of amine-functionalized solids, such as porous silicas, in which the host structure and spatial distribution of amines are often more challenging to control and characterize.<sup>30–33</sup> Specifically, we have endeavored to: (i) develop a combined NMR and DFT approach to distinguish between ammonium carbamate and carbamic acid formation, (ii) determine ranges of NMR parameters for these mechanisms so that researchers may more readily make structural assignments, (iii) understand the mixed chemisorption mechanism and unique CO<sub>2</sub> adsorption properties of (dmpn)<sub>2</sub>Mg<sub>2</sub>(dobpdc), and (iv) to investigate the effect of water on CO<sub>2</sub> chemisorption mechanisms.

## RESULTS AND DISCUSSION

**Characterization of Ammonium Carbamate Chains.** The material  $e\text{-}2\text{-Mg}_2(\text{dobpdc})$  ( $e\text{-}2 = N\text{-ethylethylenediamine}$ ) was recently proposed to form ammonium carbamate chains exclusively upon adsorption of  $\text{CO}_2$  (Figure 1c),<sup>14</sup> based on its step-shaped adsorption isotherms that saturate at a loading of one  $\text{CO}_2$  molecule per diamine, as well as infrared spectra of the  $\text{CO}_2$ -dosed material. These results were also consistent with data collected for the isostructural framework  $e\text{-}2\text{-Zn}_2(\text{dobpdc})$ , for which the formation of ammonium carbamate chains upon exposure to  $\text{CO}_2$  was also confirmed via *in situ* single-crystal X-ray diffraction experiments. We thus chose to first investigate  $e\text{-}2\text{-Mg}_2(\text{dobpdc})$  in detail with NMR spectroscopy, as a benchmark material to confirm and explore the formation of ammonium carbamate chains. Studies of gas-dosed samples were enabled by a home-built apparatus (Figure 2) that allows rotors (sample holders) for magic angle spinning (MAS) NMR experiments to be sealed at different pressures of  $^{13}\text{CO}_2$  gas (99%  $^{13}\text{C}$ ).<sup>15</sup> Following evacuation, activated samples were dosed with  $^{13}\text{CO}_2$  at a pressure of  $\sim 1$  bar that is above the adsorption step for this material at 25 °C (see Figure S1). The samples were then allowed to equilibrate before they were capped inside the manifold using a move-

able plunger. This dosing system is similar to those previously reported for studies of zeolites<sup>34</sup> and amine-functionalized silicas.<sup>35</sup>

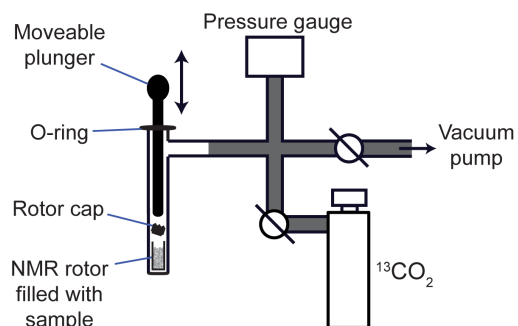


**Figure 2.** Schematic of home-built manifold for preparing gas-dosed NMR samples. The white section on the left is made from glass, and gray sections are made from stainless steel tubing. Swagelok® VCR metal gasket face seal fittings were used for steel-to-steel connections, and Swagelok® Ultra Torr fittings were used for glass-to-steel connections. Capacitance Manometers (MKS Instruments model 722B) were used for pressure measurements.

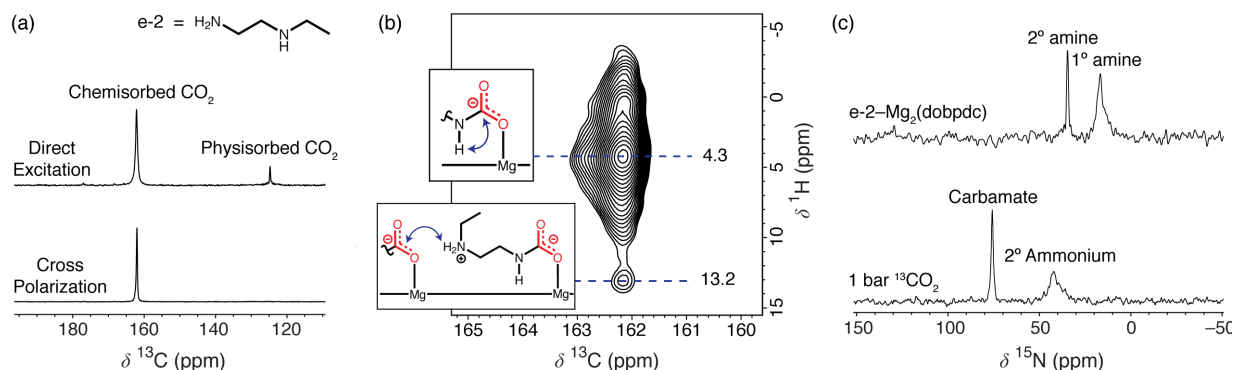


**Figure 3.** Solid-state MAS NMR (16.4 T) spectra of  $e\text{-}2\text{-Mg}_2(\text{dobpdc})\text{-CO}_2$ . (a)  $^{13}\text{C}$  NMR spectra by direct excitation (no  $^1\text{H}$  decoupling) and cross-polarization (with continuous wave decoupling of  $^1\text{H}$ ). A 1:1  $\text{CO}_2$ :diamine reaction affords a capacity of 4.0 mmol/g  $\text{CO}_2$ , which is reached above the adsorption step of the material (see Figure S1). Cross-polarization experiments allow the much faster observation of chemisorbed  $\text{CO}_2$  compared to direct excitation experiments (partly because of the long longitudinal relaxation time,  $T_1 = 60$  s, for chemisorbed  $\text{CO}_2$ ). Cross-polarization is used for the majority of  $^{13}\text{C}$  experiments that follow in this work. Note that framework and amine carbons are only weakly observed in these experiments, as they have the natural abundance of  $^{13}\text{C}$  ( $\sim 1\%$ ). (b)  $^1\text{H} \rightarrow ^{13}\text{C}$  HETCOR (contact time 100  $\mu\text{s}$ ) spectrum and correlation assignments. (c) Nitrogen-15 NMR spectra (natural isotopic abundance) of  $e\text{-}2\text{-Mg}_2(\text{dobpdc})$  before and after reaction with  $^{13}\text{CO}_2$  (1 bar). Recent X-ray crystallography of toluene-solvated  $e\text{-}2\text{-Zn}_2(\text{dobpdc})$  showed that this diamine binds to zinc(II) from the 1° amine,<sup>14</sup> with dynamics in the anticipated 1° amine–Mg interaction a likely cause of  $^{15}\text{N}$  line broadening for the 1° amine  $^{15}\text{N}$  resonance here. The magic angle spinning (MAS) rate was 15 kHz in all cases.  $^{13}\text{CO}_2$  gas dosing pressures were approximately 1 bar, and gas dosing and NMR experiments were performed at room temperature.

The  $^{13}\text{C}$  NMR spectra of  $^{13}\text{CO}_2$ -dosed  $e\text{-}2\text{-Mg}_2(\text{dobpdc})$  exhibit resonances assignable to both chemisorbed and physisorbed  $\text{CO}_2$  at 162.1 and 124.7 ppm, respectively (Figure 3a). Experiments on two independent samples (see Supporting Information, Figure S2), as well as experiments by another research group,<sup>36</sup> have shown that the  $^{13}\text{C}$  chemical shift for chemisorbed  $\text{CO}_2$  is reproducible within  $\sim 0.1$  ppm. The chemical shift of physisorbed  $\text{CO}_2$  is within 0.4 ppm of the values observed for physisorbed  $\text{CO}_2$  in various diamine-appended  $\text{Mg}_2(\text{dobpdc})$  materials (Figure S3), although the resonance is shifted by  $-3$  ppm relative to that of free gas-phase  $\text{CO}_2$  (127.7 ppm at 1 bar).<sup>28</sup> This chemical shift difference may arise in part due to aromatic ring currents in the  $\text{dobpdc}^{4-}$  linkers.<sup>37,38</sup> Quantitative  $^{13}\text{C}$  NMR indicates that at 1 bar only a small percentage (10–15%) of the adsorbed  $\text{CO}_2$  is physisorbed, and thus adsorption primarily occurs via chemisorption

at this pressure. As expected, cross-polarization from  $^1\text{H} \rightarrow ^{13}\text{C}$  revealed only the resonance from chemisorbed  $^{13}\text{CO}_2$ , as the strong  $^1\text{H}\text{-}^{13}\text{C}$  dipole–dipole couplings necessary for efficient cross-polarization are absent for the physisorbed gas.

Additional NMR experiments enabled the assignment of the chemisorbed species as ammonium carbamate, consistent with the conclusions of earlier work.<sup>14</sup> In particular, a two dimensional  $^1\text{H} \rightarrow ^{13}\text{C}$  HETCOR spectrum with a short contact time (100  $\mu\text{s}$ ) allowed detection of only those hydrogen atoms near the  $^{13}\text{C}$  nucleus of chemisorbed  $^{13}\text{CO}_2$  (Figure 3b). This spectrum shows a dominant  $^1\text{H}$  correlation at 4.3 ppm, as well as a minor correlation at 13.2 ppm. We have assigned the former to the N–H of the carbamate group (*i.e.*,  $\text{NHRCOO}^-$ ), for which a dominant correlation is anticipated because this hydrogen is the closest to the

carbamate  $^{13}\text{C}$  carbon ( $^{13}\text{C}\cdots^1\text{H} = 2.05 \text{ \AA}$ , from the DFT structure). The N–H correlation confirms reaction of  $\text{CO}_2$  with the primary amine group, rather than the secondary amine. Reaction of  $\text{CO}_2$  with the secondary amine would form a tertiary nitrogen with no attached hydrogens, and so the N–H correlation would be absent. The minor correlation at 13.2 ppm is attributed to an ammonium hydrogen ( $^{13}\text{C}\cdots^1\text{H} = 2.43 \text{ \AA}$  from DFT) and supports the formation of ammonium carbamate chains, in which carbamate and ammonium groups are ion-paired and strongly hydrogen bonded. We note that ammonium carbamate chain formation is necessary here to achieve the observed  $\text{CO}_2$  adsorption capacity of one  $\text{CO}_2$  per diamine (see Figure S1), which excludes the formation of other ammonium carbamate species

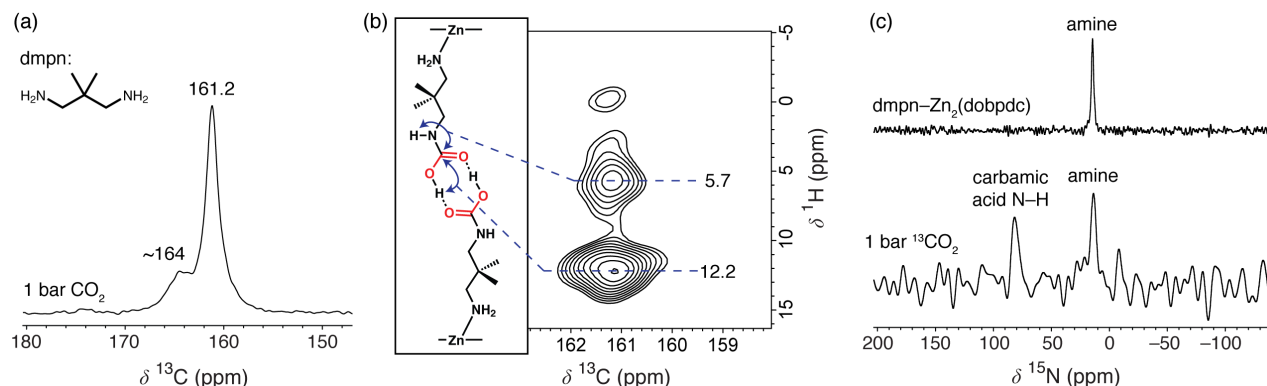


**Figure 4.** MAS NMR (16.4 T) measurements of dmpn- $\text{Zn}_2(\text{dobpdc})$  dosed with  $\text{CO}_2$  at a pressure of 1015 mbar. (a)  $^{13}\text{C}$  NMR cross-polarization spectrum (with continuous wave decoupling of  $^1\text{H}$ ). (b)  $^1\text{H} \rightarrow ^{13}\text{C}$  HETCOR (contact time 100  $\mu\text{s}$ ) spectrum and correlation assignments (the minor correlation at  $\sim 0$  ppm arises from the methyl groups on the diamine backbone). (c)  $^{15}\text{N}$  NMR (at natural isotopic abundance) cross polarization spectra (contact time 1 ms) of dmpn- $\text{Zn}_2(\text{dobpdc})$  before and after reaction with  $^{13}\text{CO}_2$ . For  $^{15}\text{N}$  NMR the acquisition times were 20 h and 8.5 h for dmpn- $\text{Zn}_2(\text{dobpdc})$  before and after  $\text{CO}_2$  dosing, respectively. The presence of a single  $^{15}\text{N}$  resonance in activated dmpn- $\text{Zn}_2(\text{dobpdc})$  suggests that the free end of the amine and the metal-bound end are likely undergoing rapid exchange under the experimental conditions.<sup>5</sup> Cross polarization kinetics and variable temperature NMR experiments should be carried out in future to further investigate diamine dynamics in diamine- $\text{M}_2(\text{dobpdc})$  materials. The magic angle spinning (MAS) rate was 15 kHz in all cases. Gas dosing and NMR experiments were performed at room temperature.

**Characterization of Carbamic Acid Pairs.** The material dmpn- $\text{Zn}_2(\text{dobpdc})$  was selected as a model system for the detailed study of carbamic acid pairs in this class of MOFs. Unlike dmpn- $\text{Mg}_2(\text{dobpdc})$ , which adsorbs  $\text{CO}_2$  by a mixed chemisorption mechanism (see below), dmpn- $\text{Zn}_2(\text{dobpdc})$  forms carbamic acid pairs when dosed at  $\text{CO}_2$  pressures close to 1 bar, as confirmed by single-crystal X-ray diffraction and  $^{13}\text{C}$  solid-state NMR spectroscopy.<sup>15</sup> Although molecular carbamic acids have also been characterized crystallographically,<sup>43</sup> this result represents the only crystallographic characterization to date of a carbamic acid pair structure in an amine-functionalized adsorbent, and so serves as a valuable model system for further study by NMR.

Figure 4a shows the  $^1\text{H} \rightarrow ^{13}\text{C}$  cross-polarization spectrum of dmpn- $\text{Zn}_2(\text{dobpdc})$  dosed with 1015 mbar of  $^{13}\text{CO}_2$ . The spectrum exhibits a major resonance at 161.2 ppm, similar to that observed in our previous work,<sup>15</sup> which we assign to carbamic acid pairs. This chemical shift is similar to those previously assigned to carbamic acids in the literature.<sup>35,40,41,44–46</sup> The weak resonance at  $\sim 164$  ppm likely arises from a minor amount of ammonium carbamate (see Figure S5). Importantly, a two dimensional  $^1\text{H} \rightarrow ^{13}\text{C}$  HETCOR experiment (short contact time) revealed two major correlations at  $^1\text{H}$  chemical shifts of 12.2 and 5.7 ppm (Figure 4b), assigned to hydrogens of the carbamic acid ( $\text{NHCOOH}$  and  $\text{NHCOOH}$ , respectively). Importantly, this result contrasts to that for the ammonium carbamate chains, where one major and one minor correlation are observed (Figure

that would result in a ratio of one  $\text{CO}_2$  per two diamines—such as dangling ammonium carbamate pairs.<sup>39</sup>

The  $^{15}\text{N}$  NMR spectrum of e-2- $\text{Mg}_2(\text{dobpdc})\text{-CO}_2$  (Figure 3c) exhibits resonances assignable to carbamate (76 ppm) and ammonium (42 ppm) groups, further supporting the formation of ammonium carbamate chains via reaction of the primary amine with  $\text{CO}_2$ . The secondary ammonium resonance is shifted by +8 ppm relative to the secondary amine resonance present in the activated material e-2- $\text{Mg}_2(\text{dobpdc})$ —similar to previous  $^{15}\text{N}$  NMR studies of ammonium carbamates.<sup>40–42</sup> Overall, our multi-nuclear NMR experiments confirm that ammonium carbamate chain formation dominates for e-2- $\text{Mg}_2(\text{dobpdc})$  and e-2- $\text{Zn}_2(\text{dobpdc})$  (Figure S4).

3b). The two strong correlations at short contact times are anticipated for carbamic acid pairs, given the relatively short C $\cdots$ H distances predicted from DFT calculations (1.95  $\text{\AA}$  for C $\cdots$ H $_{\text{COOH}}$ , and 2.01  $\text{\AA}$  for C $\cdots$ H $_{\text{NHRCOOH}}$ ). Furthermore, the  $^1\text{H}$  chemical shift of the COOH carbamic acid hydrogen is consistent with the anticipated value based on previous empirical correlations between  $^1\text{H}$  chemical shifts and O $\cdots$ O distances for O–H $\cdots$ O hydrogen bonds, whereby shorter hydrogen bonds give rise to larger chemical shifts (Figure S6).<sup>47</sup> Overall, the short contact time  $^1\text{H}\text{-}^{13}\text{C}$  correlation experiments allow carbamic acid pairs to be clearly distinguished from ammonium carbamates (Figures 3b, 4b).

The  $^{15}\text{N}$  NMR spectrum of  $\text{CO}_2$ -dosed dmpn- $\text{Zn}_2(\text{dobpdc})$  exhibits resonances at 81.7 and 13.6 ppm, assigned to the  $\text{NRHCOOH}$  nitrogen and the metal-bound amine  $\text{RNH}_2\text{-Zn}$ , respectively, as supported by the DFT calculations below. The chemical shift of the  $\text{NRHCOOH}$  nitrogen cannot be used to identify carbamic acids, because it falls within the range of values used for  $\text{NRHCOO}^-$  in ammonium carbamates (Tables 1 and 2). On the other hand, the absence of a  $^{15}\text{N}$  chemical shift change for an unreacted amine helps to distinguish carbamic acids from ammonium carbamates. The  $^{15}\text{N}$  chemical shift of the metal-bound amine is very similar to that in the activated material (14.4 ppm) (Figure 4c and Table 2). This contrasts to ammonium carbamates where larger  $^{15}\text{N}$  chemical shifts are observed for the ammonium cations than the amines in the corresponding activated materials (Figure 3c).

**Table 1.** NMR results for ammonium carbamate chains. Carbon-13 chemical shifts arising from chemisorbed CO<sub>2</sub> and key <sup>1</sup>H chemical shifts measured by short-contact time <sup>1</sup>H → <sup>13</sup>C HETCOR experiments. Values from DFT are indicated in parentheses. “–” indicates not measured/calculated. \*It is assumed that RNH<sub>3</sub><sup>+</sup> undergoes rotation on the NMR timescale, and we thus report average DFT-calculated <sup>1</sup>H chemical shifts for the three ammonium hydrogens. \*\*i-2-Mg<sub>2</sub>(dobpdc) and ee-2-Mg<sub>2</sub>(dobpdc) display two adsorption steps in their CO<sub>2</sub> isotherms.<sup>14</sup> Gas dosing pressures were approximately 1 bar in all cases at room temperature and at least 30 minutes were allowed for equilibration. Errors in the experimental chemical shifts are approximately 0.1 ppm, 0.4 ppm for <sup>13</sup>C and <sup>1</sup>H, respectively. For <sup>15</sup>N the errors are approximately 0.2 ppm and 1 ppm for carbamate and ammonium nitrogens, respectively.

Compound	Amine structure	$\delta^{13}\text{C}$ (ppm) Experiment (DFT)	$\delta^1\text{H}$ (ppm) Experiment (DFT)	$\delta^{15}\text{N}$ (ppm) Experiment (DFT)	Ref. for Experiment
e-2-Mg <sub>2</sub> (dobpdc)		162.1 (160.1)	NHRCO <sub>2</sub> <sup>-</sup> : 4.3 strong (5.7) NH <sub>2</sub> R <sub>2</sub> <sup>+</sup> : 13.2 weak (12.6)	NHRCO <sub>2</sub> <sup>-</sup> : 75.8 (86.8) NH <sub>2</sub> R <sub>2</sub> <sup>+</sup> : 42.1 (43.3)	This work
m-2-Mg <sub>2</sub> (dobpdc)		162.0 (159.5)	NHRCO <sub>2</sub> <sup>-</sup> : 4.0 strong (5.3) NH <sub>2</sub> R <sub>2</sub> <sup>+</sup> : 12.8 weak (14.2)	NHRCO <sub>2</sub> <sup>-</sup> : 75.3 (85.6) NH <sub>2</sub> R <sub>2</sub> <sup>+</sup> : 32.8 (31.5)	This work
mm-2-Mg <sub>2</sub> (dobpdc)		162.6 (159.9)	NHRCO <sub>2</sub> <sup>-</sup> : 4.8 strong (5.6) NHR <sub>3</sub> <sup>+</sup> : 14.0 weak (16.4)	NHRCO <sub>2</sub> <sup>-</sup> : – (80.4) NHR <sub>3</sub> <sup>+</sup> : – (37.5)	This work
ee-2-Mg <sub>2</sub> (dobpdc)**		162.5 (160.1)	NHRCO <sub>2</sub> <sup>-</sup> : 4.7 strong (5.7) NHR <sub>3</sub> <sup>+</sup> : 13.7 weak (16.0)	NHRCO <sub>2</sub> <sup>-</sup> : 85.0 (86.5) NHR <sub>3</sub> <sup>+</sup> : 52.7 (58.2)	This work
m-2-m-Mg <sub>2</sub> (dobpdc)		163.8 (162.4)	NH <sub>2</sub> R <sub>2</sub> <sup>+</sup> : 15.5 weak (16.0)	NR <sub>2</sub> CO <sub>2</sub> <sup>-</sup> : 73.3 (79.5) NH <sub>2</sub> R <sub>2</sub> <sup>+</sup> : 33.4 (32.9)	This work
mpn-Mg <sub>2</sub> (dobpdc)		163.1 (164.9)	NHRCO <sub>2</sub> <sup>-</sup> : 4.8 strong (4.7) NH <sub>3</sub> R <sup>+</sup> : 7.6 weak (8.2)	NHRCO <sub>2</sub> <sup>-</sup> : 86.5 (81.0) NH <sub>3</sub> R <sup>+</sup> : 33.7 (35.0)	This work
pn-Mg <sub>2</sub> (dobpdc)		162.7 (165.4)	NHRCO <sub>2</sub> <sup>-</sup> : – (6.2) NH <sub>3</sub> R <sup>+</sup> : – (8.2)	NHRCO <sub>2</sub> <sup>-</sup> : – (92.5) NH <sub>3</sub> R <sup>+</sup> : – (41.9)	[15]
dmen-Mg <sub>2</sub> (dobpdc)		163.7 (162.1)	NHRCO <sub>2</sub> <sup>-</sup> : – (4.7) NH <sub>3</sub> R <sup>+</sup> : – (8.4)	NHRCO <sub>2</sub> <sup>-</sup> : 77 (77.3) NH <sub>3</sub> R <sup>+</sup> : 51 (58.6)	[15,18]
(R,R)-dach-S-Mg <sub>2</sub> (dobpdc)		163.4 (159.6)	NHRCO <sub>2</sub> <sup>-</sup> : 4.8 strong (5.2) NH <sub>3</sub> R <sup>+</sup> : 7.2 weak (7.3*)	NHRCO <sub>2</sub> <sup>-</sup> : – (91.4) NH <sub>3</sub> R <sup>+</sup> : – (36.4)	[19]
(R,R)-dach-R-Mg <sub>2</sub> (dobpdc)	“	161.6 (159.4)	NHRCO <sub>2</sub> <sup>-</sup> : 3.9 strong (4.1) NH <sub>3</sub> R <sup>+</sup> : 7.8 weak (7.6*)	NHRCO <sub>2</sub> <sup>-</sup> : – (98.7) NH <sub>3</sub> R <sup>+</sup> : – (37.1)	[19]
i-2-Mg <sub>2</sub> (dobpdc)**		163.3, 162.5, 161.9 (161.5)	NHRCO <sub>2</sub> <sup>-</sup> : 4.4 strong (5.8) NH <sub>2</sub> R <sub>2</sub> <sup>+</sup> : 12-13 weak (13.6)	NHRCO <sub>2</sub> <sup>-</sup> : – (75.8) NH <sub>2</sub> R <sub>2</sub> <sup>+</sup> : – (57.5)	This work



**Table 2.** NMR results for carbamic acid pairs. As for Table 1, except data reflect carbamic acid pairs. Values from vdW-corrected DFT calculations are indicated in parentheses. The gas dosing pressure was 1015 mbar, with gas dosing carried out at room temperature. Note: dmpn-Zn<sub>2</sub>(dobpdc) undergoes a different (mixed) mechanism at lower pressures (see below).

Compound	Amine structure	$\delta^{13}\text{C}$ (ppm) Experiment (DFT)	$\delta^1\text{H}$ (ppm) Experiment (DFT)	$\delta^{15}\text{N}$ (ppm) Experiment (DFT)
dmpn-Zn <sub>2</sub> (dobpdc)		161.2 (162.3)	COOH: 12.2 strong, (14.5) NHCO <sub>2</sub> H: 5.7 strong, (7.6)	NHRCO <sub>2</sub> H: 81.7 (90.8) Zn-NH <sub>2</sub> R: 13.6 (9.9)

We performed similar NMR measurements on a series of diamine-appended Mg<sub>2</sub>(dobpdc) materials in which the diamine was varied (Table 1). All of the materials exhibit step-shaped CO<sub>2</sub> adsorption isotherms,<sup>14,15,19</sup> and were studied under CO<sub>2</sub> pressures much greater than the step pressure. Under these conditions, the materials listed in Table 1 all display NMR spectra consistent with the formation of ammonium carbamate chains (Figures S7-S9), supporting the hypothesis that this mechanism dominates for a wide range of diamines.<sup>14,15,19</sup> The key evidence for ammonium carbamate chain formation is the observation of <sup>13</sup>C resonances that correlate strongly with a carbamate N-H group and weakly with an ammonium group in two-dimensional experiments. The observation of ammonium resonances in the <sup>15</sup>N NMR spectra provides additional support for ammonium carbamate chain formation. Additionally, the measured chemical shifts generally show good agreement with DFT-calculated values for ammonium carbamate chain structures (see below). For additional discussion on m-2-Zn<sub>2</sub>(dobpdc) and i-2-Mg<sub>2</sub>(dobpdc), see Figures S7 and S10, respectively.

The large <sup>1</sup>H chemical shifts of the ammonium resonances (15.1–7.2 ppm) are consistent with the formation of hydrogen-bonded ion pairs.<sup>14</sup> The secondary and tertiary ammonium <sup>1</sup>H chemical shifts (15.1–12.3 ppm) are well predicted by our 0 K DFT calculations, indicating that the alkyl ammonium groups do not rotate significantly on a millisecond timescale, likely due to steric restrictions within the pores of the material. In contrast, for primary ammonium groups (RNH<sub>3</sub><sup>+</sup>), smaller chemical shifts of 7–8 ppm are observed, together with somewhat stronger resonances. Averaging of the DFT-calculated values for the three different H at-

oms was required to obtain reasonable agreement between calculation and experiment, suggesting that these primary ammonium groups do rotate on the NMR timescale. An average of calculated <sup>1</sup>H chemical shifts for RNH<sub>3</sub><sup>+</sup> groups was also shown to result in agreement between experiment and theory in previous studies of glycine in the solid state, where room temperature rotation of RNH<sub>3</sub><sup>+</sup> groups is known.<sup>48,49</sup> In the  $\alpha$  and  $\gamma$  polymorphs of glycine, the <sup>1</sup>H chemical shifts for the RNH<sub>3</sub><sup>+</sup> group are 8.4 and 8.8 ppm, respectively,<sup>48</sup> similar to the <sup>1</sup>H chemical shifts measured here for the primary ammonium cations.

The foregoing spectral assignments are well-supported by vdW-corrected DFT calculations of <sup>1</sup>H, <sup>13</sup>C, and <sup>15</sup>N chemical shifts (Figure 5). Note that vdW-corrections are important for the accurate computational treatment of adsorption (and related) properties of MOFs.<sup>5,24,25</sup> For the <sup>1</sup>H NMR spectra, good agreement is achieved between experimental and calculated chemical shifts for both the N-H carbamate (NHRCO<sub>2</sub><sup>-</sup>) and the ammonium (NHR<sub>3</sub><sup>+</sup>) protons (Figure 5a), with a total root mean square deviation (RMSD) of 1.3 ppm between experiment and theory. The calculated and experimental <sup>13</sup>C chemical shift values have a slightly higher RMSD of 2.2 ppm, with the largest deviations approaching 3 ppm (Figure 5b). While this agreement is good given the large <sup>13</sup>C chemical shift range (~200 ppm), the discrepancies between experiment and theory are of similar order to the range of <sup>13</sup>C chemical shifts for different forms of chemisorbed CO<sub>2</sub> (~4 ppm, Tables 1 and 2). The RMSD value of 6.3 ppm for <sup>15</sup>N is small compared to the large chemical shift range of this nucleus (~900 ppm).

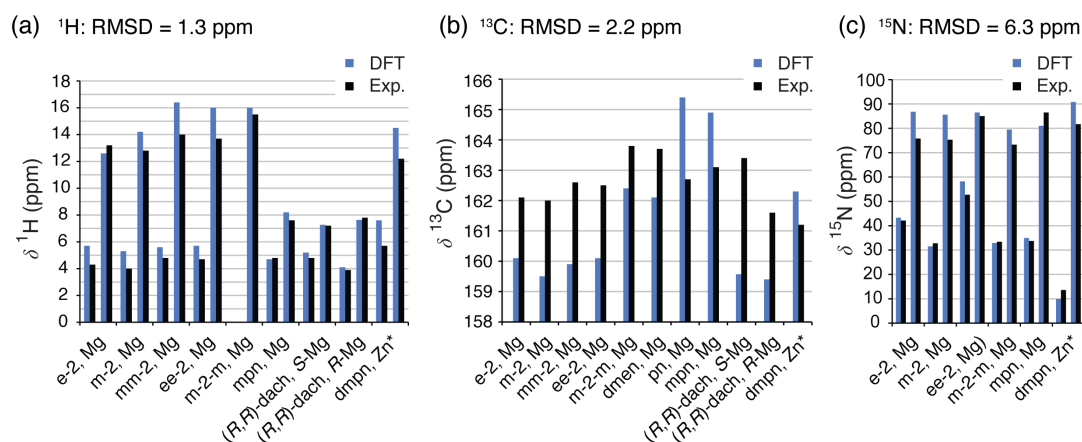


**Figure 5.** Key experimental and vdW-corrected DFT-calculated chemical shifts for diamine-M<sub>2</sub>(dobpdc) compounds following chemisorption of CO<sub>2</sub> at approximately 1 bar at room temperature for at least 30 minutes. The overall root mean square deviations are given for each nucleus to quantify the typical discrepancies between experimental and DFT values. \*Note that all compounds in this figure form ammonium carbamate chains, except for dmpn-Zn<sub>2</sub>(dobpdc), which forms carbamic acid pairs. M<sub>2</sub>(dobpdc) is chiral and racemates were studied in all cases except for where indicated with S or R labels. For <sup>1</sup>H (a), left and right bars correspond to chemical shifts of the NHCOO<sup>-</sup> and NR<sub>3</sub>H<sup>+</sup> groups, respectively, with the exception of

dmpn-Zn<sub>2</sub>(dobpdc), where the right bar is the carbamic acid NR<sub>2</sub>COOH hydrogen. For <sup>13</sup>C (b) the chemical shift of the carbamate (NR<sub>2</sub>COO<sup>-</sup>) carbon is given, except for dmpn-Zn<sub>2</sub>(dobpdc), where the chemical shift of the carbamic acid (NR<sub>2</sub>COOH) carbon is given. For <sup>15</sup>N (c), left and right bars for each compound correspond to ammonium (NR<sub>3</sub>H<sup>+</sup>) and carbamate (NH<sub>2</sub>COO<sup>-</sup>) nitrogen atoms, respectively, except for dmpn-Zn<sub>2</sub>(dobpdc), where left and right bars correspond to metal-bound amine (M-NR<sub>2</sub>) and carbamic acid (NR<sub>2</sub>COOH) nitrogen atoms, respectively.

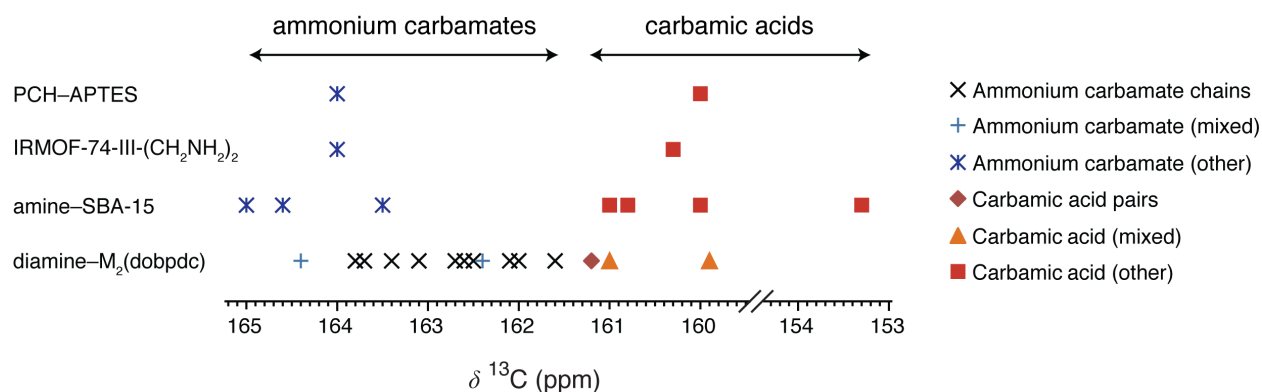


**Figure 6.** Summary of reported <sup>13</sup>C chemical shifts for chemisorbed CO<sub>2</sub> species in amine-functionalized adsorbents. Data for diamine-M<sub>2</sub>(dobpdc) samples are from this work and Refs 15 and 19; data for amine-functionalized SBA-15 materials are from Refs 35, 41, and 45; data for IRMOF-74-III-(CH<sub>2</sub>NH<sub>2</sub>)<sub>2</sub> are from Ref<sup>40</sup>; and data for PCH-APTES (porous clay heterostructure functionalized with 3-aminopropyltriethoxysilane) are from Ref<sup>44</sup>. For discussion of mixed chemisorption structures, see below.

Overall our results indicate that the ammonium carbamate chain formation dominates for diamine-M<sub>2</sub>(dobpdc) materials with diverse diamine structures, in agreement with previous work.<sup>5,14,15,17,18</sup> A range of <sup>13</sup>C chemical shifts from 161.6–163.8 ppm is observed for ammonium carbamate chains in these materials (Table 1, Figure 6), and the observed <sup>13</sup>C chemical shift of 161.2 ppm for carbamic acid pairs falls just outside of this range (Table 2). Factors such as the number of alkyl groups on the nitrogen atom and the presence of backbone alkyl groups can affect the <sup>13</sup>C chemical shifts for ammonium carbamate chains, while stereochemistry can also play a role for diastereomeric compounds—M<sub>2</sub>(dobpdc) is chiral and forms as a racemate under typical synthetic conditions.<sup>19</sup>

The <sup>13</sup>C chemical shifts for chemisorbed species in diamine-appended M<sub>2</sub>(dobpdc) materials, as well as other amine-functionalized adsorbents from the literature<sup>35,40,41,44,45</sup> are shown in Figure 6. The new data for diamine-M<sub>2</sub>(dobpdc) materials extends the known ranges of <sup>13</sup>C chemical shifts for ammonium carbamates and carbamic acids. Because the shift ranges for ammonium carbamate and carbamic acid species nearly overlap (Figure 6), the use of <sup>13</sup>C NMR spectroscopy alone should be

treated with significant caution when making judgments regarding chemisorption mechanisms in amine-functionalized materials, especially given the RMSD value of 2.2 ppm between experimental and calculated <sup>13</sup>C chemical shift values. As a further note of caution, ammonium bicarbonate formation was recently observed following CO<sub>2</sub> adsorption in amine functionalized mesoporous silicas under wet conditions, with corresponding <sup>13</sup>C chemical shifts (162–163 ppm) falling within range of those observed for the ammonium carbamate species identified here.<sup>50,51</sup> Similar to the <sup>13</sup>C chemical shifts, the <sup>15</sup>N chemical shifts measured here also show variation from compound to compound, further illustrating the importance of additional NMR experiments beyond 1D <sup>13</sup>C and <sup>15</sup>N spectra to obtain conclusive mechanistic assignments. Indeed, recent work on amine-functionalized silicas has shown that the use of the anisotropy of the <sup>13</sup>C chemical shift (rather than simply isotropic chemical shifts) can enable identification of neutral versus charged chemisorption products.<sup>52</sup> Overall, these studies demonstrate that <sup>1</sup>H, <sup>13</sup>C, and <sup>15</sup>N NMR experiments, combined with DFT calculations, provide far more reliable structural assignments than 1D NMR experiments and calculations on a single nucleus.

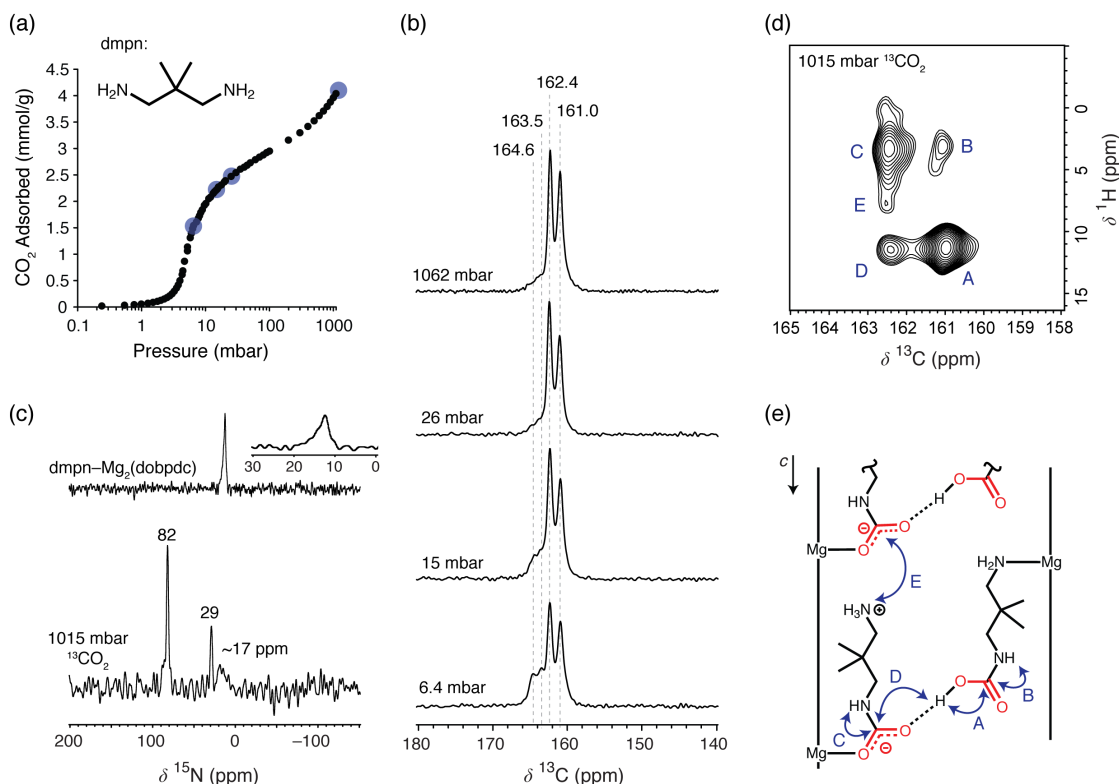


**Figure 7.** (a) CO<sub>2</sub> adsorption isotherm of dmpn-Mg<sub>2</sub>(dobpdc) at 25 °C; data taken from our previous work (Note: a 1:1 CO<sub>2</sub>:diamine reaction gives 3.8 mmol of adsorbed CO<sub>2</sub> per gram of material, which is reached at pressure close to 1 bar CO<sub>2</sub>).<sup>15</sup> (b) MAS <sup>13</sup>C NMR (16.4 T) spectra acquired by cross polarization (contact time 1 ms) for dmpn-Mg<sub>2</sub>(dobpdc)-CO<sub>2</sub> samples dosed at different gas pressures, which are approximated by blue circles on the gas adsorption isotherm in a). (c) <sup>15</sup>N NMR spectra acquired by cross-polarization from <sup>1</sup>H (contact time 1 ms). An enlarged inset is shown for dmpn-Mg<sub>2</sub>(dobpdc), with a broad asymmetric feature that could be deconvoluted into two resonances at 14 and 12 ppm, suggesting that the exchange of the metal-bound and free ends of the diamine is slower than in dmpn-Zn<sub>2</sub>(dobpdc) (Figure 4c). (d) <sup>1</sup>H → <sup>13</sup>C HETCOR (contact time 100 μs) spectrum for dmpn-Mg<sub>2</sub>(dobpdc)-CO<sub>2</sub> dosed at 1015 mbar. (e) Portion of the proposed structure (see Figure 8) with key <sup>1</sup>H – <sup>13</sup>C HETCOR correlations indicated by blue arrows and labels A–E. Gas dosing times were >13 hours in all cases, and care was taken to avoid air exposure between sample activation and gas dosing, as water vapor has a large effect on the chemisorption mechanism (see below). Gas dosing and NMR experiments were performed at room temperature.

**A Mixed Chemisorption Mechanism.** Having established NMR parameters to distinguish between ammonium carbamate chains and carbamic acid pairs, we next studied the apparent mixed chemisorption mechanism in dmpn-Mg<sub>2</sub>(dobpdc).<sup>15</sup> The 25 °C CO<sub>2</sub> adsorption isotherm for this material is shown in Figure 7a, and <sup>13</sup>C NMR spectra collected at various gas dosing pressures are shown in Figure 7b. At all pressures, the <sup>13</sup>C NMR spectrum is dominated by two main resonances at 162.4 and 161.0 ppm, while two minor features are also present at ~164.6 and ~163.5 ppm at lower pressures (Figure 7b). These results suggest a different chemisorption mechanism from that resulting in the formation of only carbamic acid pairs, as observed for dmpn-Zn<sub>2</sub>(dobpdc) at CO<sub>2</sub> pressures close to 1 bar (Figure 4). The major <sup>13</sup>C resonances at 162.4 and 161.0 ppm are assigned to ammonium carbamate and carbamic acid, respectively, on the basis of data in Tables 1 and 2. Following dosing with <sup>13</sup>CO<sub>2</sub> at 1015 mbar, the <sup>15</sup>N NMR spectrum of dmpn-Mg<sub>2</sub>(dobpdc) exhibits an ammonium resonance at 29 ppm (similar to the ammonium resonance in the related material mpn-Mg<sub>2</sub>(dobpdc), see Table 1) and a broad resonance at ~17 ppm, which we assign to a metal-bound amine (Figure 7c). The <sup>15</sup>N NMR spectrum was reproducible for two independent samples (Figure S11), and provides additional evidence for the formation of a mixture of ammonium carbamate and carbamic acid. Only a single reso-

nance could be observed for NHCOO<sup>−</sup>/NHCOOH species, likely due to their similar chemical shift values.<sup>42,45</sup>

The assignment of the <sup>13</sup>C resonance at 161.0 ppm to carbamic acid is further supported by data from <sup>1</sup>H → <sup>13</sup>C HETCOR experiments at a short contact time of 100 μs (Figure 7d), which show a strong <sup>1</sup>H correlation assignable to the COOH group (<sup>1</sup>H 11.3 ppm, correlation A) and a correlation from a NHRCOOH group (<sup>1</sup>H 3.1 ppm, correlation B). The <sup>13</sup>C resonance at 162.4 ppm shows a strong NHCOO<sup>−</sup> correlation (<sup>1</sup>H 3.3 ppm, correlation C), and surprisingly the carbamate carbon also shows a correlation with the carbamic acid COOH group (correlation D), although this correlation is weaker than it is for the 161.0 ppm <sup>13</sup>C resonance. The latter correlation indicates that the hydrogen of the carbamic acid –OH group is near the carbon of the assigned ammonium carbamate (Figure 7e). Interestingly, the ratio of the integrated areas of the two main resonances (as determined by quantitative <sup>13</sup>C NMR experiments) was found to be 1:1.0 and 1:0.9 (left resonance:right resonance) at pressures of 1015 and 26 mbar, respectively, suggesting that the two species are present in nearly equal amounts over this pressure range. Notably, a similar mixed chemisorption behavior was also observed for dmpn-Zn<sub>2</sub>(dobpdc) at intermediate gas-dosing pressures—*i.e.*, above the adsorption step but below the pressures where conversion to carbamic acid pairs occurs (see Figure S10). At lower gas pres-



tures of 15 and 6.4 mbar, two additional minor resonances are clearly seen for  $\text{dmpn-Mg}_2(\text{dobpdc})$  at  $\sim 164.6$  and  $163.5$  ppm (Figure 7b), assigned to ammonium carbamate species that are not interacting with carbamic acids (see Figure S13).

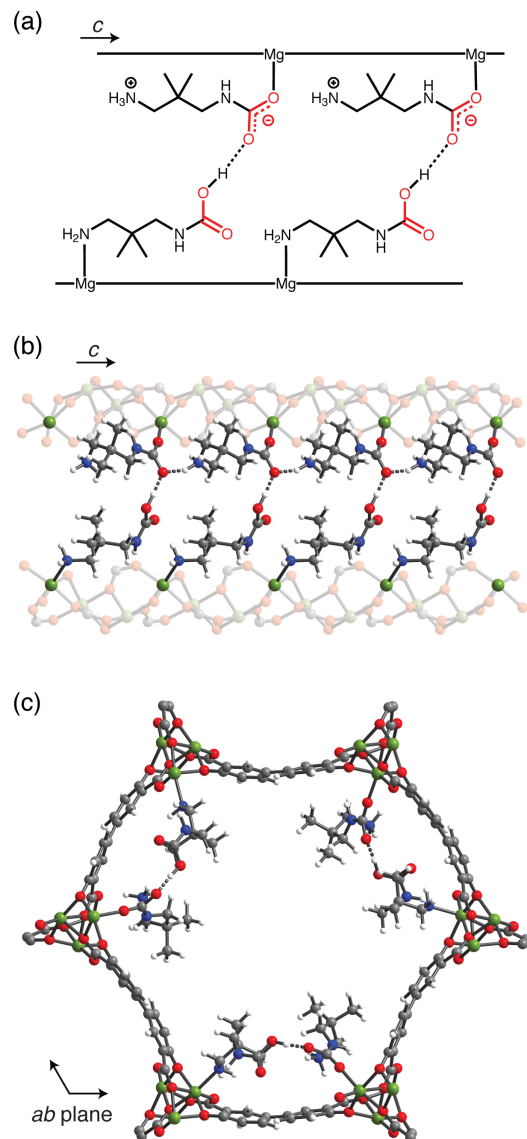


**Figure 8.** Proposed mixed chemisorption structure with ammonium carbamate and carbamic acid in a 1:1 ratio for  $\text{dmpn-Mg}_2(\text{dobpdc})$ . a) Lewis structure. b), c) Structure from DFT calculations shown for two adjacent chains along the  $c$  axis (b) and for a projection in the  $ab$  plane (c).

Overall, the NMR data for  $\text{dmpn-Mg}_2(\text{dobpdc})$  at  $\text{CO}_2$  pressures close to 1 bar point toward a dominant new chemisorption mechanism with a 1:1 ratio of interacting ammonium carbamate and carbamic acid species. Guided by our NMR results, a vdW-corrected DFT survey of structures with a 1:1 ratio of ammonium carbamate and carbamic acid led to the discovery of the structure shown in Figure 8. Here, ammonium carbamate chains and carbamic acid chains propagate along the  $c$  axis, down the one-dimensional channels of the framework. Hydrogen bonds are present in the ammonium carbamate chain and also across the  $ab$  plane between the carbamic acid hydrogen and the neighboring, unbound oxygen atom of the carbamate, forming an extended

ladder-like structure (Figure 8b). Our calculated chemical shifts for this structure are in good agreement with experimental  $^1\text{H}$  NMR shifts (Table 3), with a total RMSD of 1.3 ppm for the four assigned  $^1\text{H}$  resonances. This proposed mixed chemisorption structure notably serves to explain the key  $^1\text{H}$ - $^{13}\text{C}$  correlations observed in the HETCOR experiments (Figure 7c): the major correlation of the carbamic acid carbon to an acid  $-\text{OH}$  (correlation A, Figure 7c) is anticipated given the short  $\text{C}_{\text{COOH}}\cdots\text{H}_{\text{COOH}}$  distance of  $1.94 \text{ \AA}$  in the DFT-derived structure, as is the weak correlation of the  $\text{COOH}$  hydrogen resonance with the ammonium carbamate carbon (correlation D,  $\text{C}_{\text{NHCOO}^-}\cdots\text{H}_{\text{COOH}}$  distance of  $2.59 \text{ \AA}$ ). This mixed structure also accounts for the apparent 1:1 ratio of these chemisorption products, with synergistic ammonium carbamate and carbamic acid formation owing to the hydrogen bonding between these groups.

Finally, Rietveld refinement of powder X-ray diffraction data of  $\text{CO}_2$ -dosed  $\text{dmpn-Mg}_2(\text{dobpdc})$  was carried out, using the DFT structure (Figure 8) as a starting point (Figures S14 and S15, Tables S1 and S2). Good agreement was obtained, though slight discrepancies were observed between the simulated and experimental diffraction pattern, which appear to be due to some disorder of the alkyl groups of the amine that could not be modeled. Rietveld refinement using a pure ammonium carbamate structural model from DFT showed a worse agreement to the data than the mixed chemisorption structure.



To further explore the observed chemisorption products, we used DFT to calculate the  $\text{CO}_2$  adsorption energies ( $\Delta E_{\text{ads}}$ ) associated with their formation (Table 4). Recent vdW-corrected DFT calculations have accurately predicted  $\Delta E_{\text{ads}}$  for  $\text{CO}_2$  adsorption in diamine- $\text{M}_2(\text{dobpdc})$  materials.<sup>20,24,26,27</sup> The experimental adsorption enthalpy for  $\text{CO}_2$  in  $\text{dmpn-Mg}_2(\text{dobpdc})$  was determined to be approximately  $-70 \text{ kJ/mol}$  at gas loadings ranging from 0–2.8 mmol/g, and this value decreased to about  $-53 \text{ kJ/mol}$  at a  $\text{CO}_2$  loading of 3.2 mmol/g.<sup>15</sup> The mixed chemisorption structure introduced above is calculated to have  $\Delta E_{\text{ads}} = -54 \text{ kJ/mol}$  (for full  $\text{CO}_2$  capacity, *i.e.*, 1  $\text{CO}_2$  molecule per diamine, see Table 4), agreeing with the heat of adsorption determined at the highest experimental loading. The calculated value is very slightly larger in magnitude than that predicted for carbamic acid pairs ( $\Delta E_{\text{ads}} = -53 \text{ kJ/mol}$ ), which are not observed experimentally in  $\text{dmpn-Mg}_2(\text{dobpdc})$ . Additional DFT calculations of a pure ammonium carbamate chain structure yielded  $\Delta E_{\text{ads}} = -69 \text{ kJ/mol}$ , which is 15 kJ/mol larger in magnitude than that for the mixed structure. While DFT predicts the pure ammonium carbamate chain structure to be the most enthalpically favored at full  $\text{CO}_2$  loading (*i.e.*, at  $\sim 1 \text{ bar CO}_2$ ), our experimental NMR data clearly exclude a pure ammonium carbamate mechanism under these conditions (Figure 7). Kinetic or entropic effects,<sup>53</sup> which are not accounted for in the DFT calculations, may partly explain the discrepancy between the calculated adsorption energies and the structures observed by NMR spectroscopy.

At  $\text{CO}_2$  pressures below 1 bar, the NMR results (Figure 7b) reveal a combination of ammonium carbamate chains and the mixed chemisorption structure (carbamic acid–ammonium carbamate adducts). Interestingly, at 50%  $\text{CO}_2$  capacity, DFT calculations predict a possible structure containing 2/3 ammonium carbamates and 1/3 carbamic acids (Figure S16 with  $\Delta E_{\text{ads}} = -73 \text{ kJ/mol}$ , close to the heat of adsorption determined at the corresponding experimental  $\text{CO}_2$  loading. Note that to obtain equi-

brated samples, we dosed freshly activated dmpn-Mg<sub>2</sub>(dobpdc) for at least 13 h. Shorter dosing times (as well as wet conditions, see below) resulted in larger amounts of ammonium carbamate species not interacting with carbamic acid (based on <sup>13</sup>C NMR data; see Figure S17), suggesting that ammonium carbamate chains are the kinetic product, while the mixed structure is the

thermodynamic product. Finally, the carbamic acid pairs appear to be the most enthalpically favored chemisorption structure at the maximum CO<sub>2</sub> loading (Table 4) in dmpn-Zn<sub>2</sub>(dobpdc), consistent with the observation of these species at high dosing pressures by NMR and X-ray diffraction.<sup>15</sup>

**Table 3. Experimental and vdW-corrected DFT-calculated chemical shifts for the proposed mixed structure shown in Figure 8. See Figure S12 and the subsequent discussion for dmpn-Zn<sub>2</sub>(dobpdc).**

Compound	Amine structure	$\delta^{13}\text{C}$ (ppm) Experiment (DFT)	$\delta^1\text{H}$ (ppm) Experiment (DFT)	$\delta^{15}\text{N}$ (ppm) Experiment (DFT)
dmpn-Mg <sub>2</sub> (dobpdc)		COO <sup>-</sup> : 162.4 (158.5) COOH: 161.0 (157.4)	COOH: 11.3 strong, (12.1) NHCO <sub>2</sub> H: 3.1 strong, (4.7) NHCO <sub>2</sub> <sup>-</sup> : 3.3 strong, (4.5) NH <sub>3</sub> R: 7.2 weak (8.5)	NHRCO <sub>2</sub> H: 82* (64.8) Zn-NH <sub>2</sub> R: 17 (12.1) NHRCO <sub>2</sub> <sup>-</sup> : 82* (98.9) NH <sub>3</sub> R <sup>+</sup> : 29 (25.6)
dmpn-Zn <sub>2</sub> (dobpdc)		COO <sup>-</sup> : 164.4 (158.1) COOH: 159.9 (158.1)	COOH: 14.3 strong, (12.2) NHCO <sub>2</sub> H: 6.0 strong, (5.7) NHCO <sub>2</sub> <sup>-</sup> : 7.3 strong, (3.8)	NHRCO <sub>2</sub> H: - (83.6) Zn-NH <sub>2</sub> R: - (12.9) NHRCO <sub>2</sub> <sup>-</sup> : - (80.4) NH <sub>3</sub> R <sup>+</sup> : - (25.8)

\*Separate NHRCO<sub>2</sub>H and NHRCO<sub>2</sub><sup>-</sup> resonances could not be identified, likely due to the overlap of these resonances.

**Table 4. vdW-corrected DFT-calculated  $\Delta E_{\text{ads}}$  values for CO<sub>2</sub> adsorption in dmpn-M<sub>2</sub>(dobpdc) compounds. The calculations assume a CO<sub>2</sub> capacity of 1 CO<sub>2</sub> per diamine. See Figure S12 for a discussion on dmpn-Zn<sub>2</sub>(dobpdc).**

Compound	Structure	$\Delta E_{\text{ads}}$ (kJ/mol)
dmpn-Mg <sub>2</sub> (dobpdc)	Mixed	-54
	Ammonium carbamate chains	-69
	Carbamic acid pairs	-53
dmpn-Zn <sub>2</sub> (dobpdc)	Mixed	-39
	Ammonium carbamate chains	-43
	Carbamic acid pairs	-53

The mixed chemisorption mechanism proposed for CO<sub>2</sub> in dmpn-Mg<sub>2</sub>(dobpdc) yields interacting ammonium carbamate and carbamic acid chains in the *ab* plane (Figure 8). To explore the role of these interactions in driving the mixed product formation, we sought to increase the distance between adsorption sites in the *ab* plane by studying CO<sub>2</sub> adsorption in dmpn-Mg<sub>2</sub>(dotpdc) (dotpdc<sup>4-</sup> = 4,4'-dioxido-[1,1':4',1''-terphenyl]-3,3''-dicarboxylate). The key structural difference between Mg<sub>2</sub>(dobpdc) and Mg<sub>2</sub>(dotpdc) is the larger minimum M...M distance across the *ab* plane—approximately 15 Å for Mg<sub>2</sub>(dotpdc) compared to ~10 Å in Mg<sub>2</sub>(dobpdc).<sup>54</sup> Importantly, the distance between metal centers along the *c* axis is anticipated to be very similar in both frameworks.<sup>16</sup>

The CO<sub>2</sub> adsorption profile of dmpn-Mg<sub>2</sub>(dotpdc) is broad compared to that of dmpn-Mg<sub>2</sub>(dobpdc), which suggests a primarily non-cooperative adsorption mechanism (Figure 9a). Indeed, NMR characterization of dmpn-Mg<sub>2</sub>(dotpdc) (Figure 9b,c) revealed a complex mixture of ammonium carbamate and carbamic acid species, quantified overall in a 1:0.5 ratio, respectively, rather than the 1:1 mixed structure observed for dmpn-Mg<sub>2</sub>(dobpdc). We note that sharp CO<sub>2</sub> adsorption isotherm steps

have been observed previously for a range of diamine-appended M<sub>2</sub>(dotpdc) variants, including *n*Pr-2-Mg<sub>2</sub>(dotpdc) (*n*Pr-2 = *N*-propylethylenediamine),<sup>16</sup> indicating that such materials are capable of cooperative adsorption by ammonium carbamate chain formation. Indeed, NMR measurements of *n*Pr-2-Mg<sub>2</sub>(dotpdc) were fully consistent with the exclusive formation of ammonium carbamate chains (Figure S18). Overall, our additional experiments on dmpn-Mg<sub>2</sub>(dotpdc) indicate that interactions between chemisorbed species in the *ab* plane of dmpn-Mg<sub>2</sub>(dobpdc) are an important feature of the mixed cooperative mechanism, lending additional support to the structure proposed in Figure 8.

The bulky methyl groups on the diaminopropane backbone of dmpn offer a means to alter the chemisorption mechanisms and the resulting thermodynamics for diamine-M<sub>2</sub>(dobpdc) materials. Notably, our results help to explain the previously measured<sup>15</sup> larger entropic penalty associated with CO<sub>2</sub> chemisorption in dmpn-Mg<sub>2</sub>(dobpdc) compared to the penalty in materials that form only ammonium carbamate chains. Indeed, the interactions between ammonium carbamates and carbamic acids in the mixed structure presumably result in additional entropy penalties. The results obtained here also help to explain the isotherm (and isobar) shape observed for dmpn-Mg<sub>2</sub>(dobpdc), which features a less sharp adsorption step than typical diamine-Mg<sub>2</sub>(dobpdc) materials.<sup>15</sup> At pressures associated with the step region, a mixture of ammonium carbamate and carbamic acid forms and hinders the full cooperative adsorption process that would result upon exclusive ammonium carbamate chain formation. The mixed mechanism may also account for the hysteresis observed upon desorption (Figure 9a), corresponding to retention of approximately 50% of the adsorbed CO<sub>2</sub>.<sup>15</sup> We tentatively propose that the CO<sub>2</sub> molecules bound as carbamic acids in the mixed structure are more easily removed upon desorption than the CO<sub>2</sub> molecules bound within ammonium carbamate chains, and that the ammonium carbamates thus account for the desorption hysteresis. Additional adsorption and desorption experiments showed that this hysteresis is most pronounced as equilibrium conditions

are approached, suggesting that the mixed chemisorption struc-

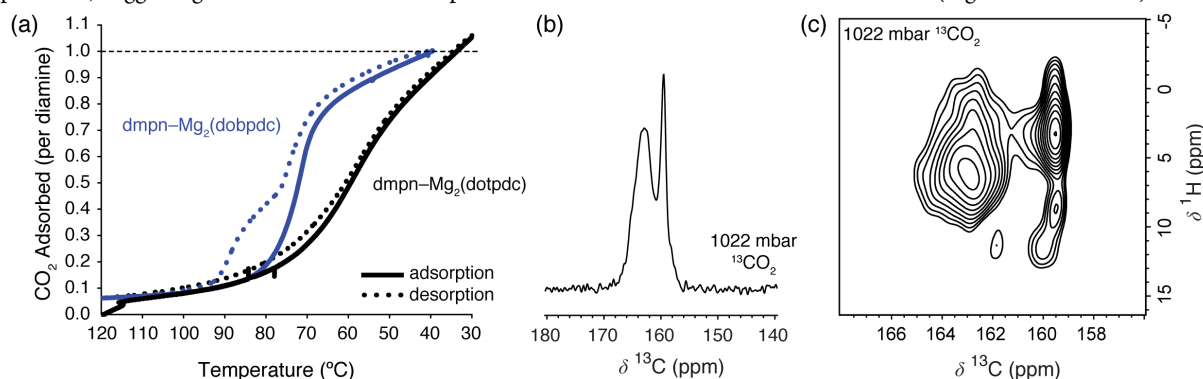


**Figure 9.** a) CO<sub>2</sub> isobars for dmpn-Mg<sub>2</sub>(dobpdc) and the expanded analogue dmpn-Mg<sub>2</sub>(dotpdc) collected by thermogravimetric analysis at atmospheric pressure using a temperature ramp rate of 1 °C/min. Solid lines show adsorption, dotted lines show desorption. The dashed line shows the theoretical capacity, and depict the two MOF structures featuring different pore sizes and shapes). b), c) Magic angle spinning NMR (16.4 T) characterization of dmpn-Mg<sub>2</sub>(dotpdc)-CO<sub>2</sub> (gas dosing pressure 1022 mbar). b) <sup>13</sup>C cross-polarization experiment (1 ms contact time). c) Short contact time (100 μs) <sup>1</sup>H → <sup>13</sup>C HETCOR experiment. As with dmpn-Mg<sub>2</sub>(dobpdc), a long gas dosing time was used (here 14 h) before sealing the rotor. MAS rate 15 kHz. NMR experiments and gas dosing were performed at room temperature.

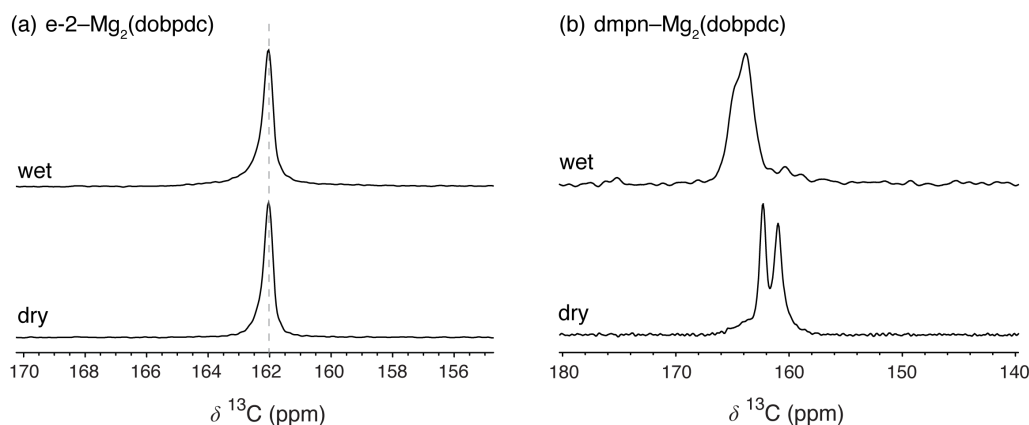


**Figure 10.** <sup>13</sup>C MAS NMR (16.4 T) experiments to investigate the role of water in directing CO<sub>2</sub> chemisorption for (a) e-2-Mg<sub>2</sub>(dobpdc) and (b) dmpn-Mg<sub>2</sub>(dobpdc). For wet experiments the sample was first exposed to wet N<sub>2</sub> for 30 min before dosing with dry <sup>13</sup>CO<sub>2</sub>. For dry experiments, freshly activated samples were dosed directly with <sup>13</sup>CO<sub>2</sub>. Gas dosing pressures were approximately 1 bar, and the MAS rate was 15 kHz for all measurements. Gas dosing and NMR experiments were performed at room temperature.

**The Role of Water in Directing Chemisorption.** Given that water vapor is present in most practical gas mixtures of interest and that all of the measurements presented so far were performed under dry conditions, it is critical to evaluate the effect of water on the chemisorption mechanisms in diamine-Mg<sub>2</sub>(dobpdc) materials. We first chose to study e-2-Mg<sub>2</sub>(dobpdc), which exclusively forms ammonium carbamate chains as discussed above (Figure 10a). At room temperature, activated e-2-Mg<sub>2</sub>(dobpdc) was first exposed to wet N<sub>2</sub> for 30 min before dosing with dry <sup>13</sup>CO<sub>2</sub> for an additional 30 min. Proton NMR data collected before and after dosing with wet N<sub>2</sub> confirmed the adsorption of water in the material (Figure S20), and <sup>13</sup>C NMR data revealed a spectrum very similar to that obtained under dry conditions, with a single resonance at 162.0 ppm assigned to ammonium carbamate chains. Separate experiments in which e-2-Mg<sub>2</sub>(dobpdc) was first exposed to dry <sup>13</sup>CO<sub>2</sub> and then wet CO<sub>2</sub> at natural isotopic abundance gave very similar results (Figure S21). These results suggest that ammonium carbamate chains can form and persist in the presence of water, which is essential for the practical application of these materials. Our results also help to explain previous studies of diamine-Mg<sub>2</sub>(dobpdc) materials, wherein

measurements under dry and humid conditions resulted in similar step-like adsorption profiles and CO<sub>2</sub> adsorption capacities.<sup>16,39</sup> Recent DFT calculations have suggested that ammonium carbamate chains are stabilized by the presence of water via hydrogen bonding interactions, indicating that water may have a beneficial effect on the CO<sub>2</sub> capture performance of these materials.<sup>24</sup>

In contrast to e-2-Mg<sub>2</sub>(dobpdc), dmpn-Mg<sub>2</sub>(dobpdc) undergoes a dramatic change in its chemisorption mechanism in the presence of water (Figure 10b). At room temperature, activated dmpn-Mg<sub>2</sub>(dobpdc) was exposed to wet N<sub>2</sub> for 30 min before dosing with <sup>13</sup>CO<sub>2</sub> for 15 h. Under wet conditions, the major chemisorption products are assigned to ammonium carbamate chains on the basis of the observed <sup>13</sup>C chemical shifts and a two dimensional HETCOR spectrum, which indicates at least two different ammonium carbamate conformations (Figure S22). This result deviates from that observed under dry conditions, wherein the mixed chemisorption structure dominates at the same gas pressures (Figure 10b). Despite the change of the chemisorption mechanism under wet conditions, the CO<sub>2</sub> adsorption capacity is maintained in dmpn-Mg<sub>2</sub>(dobpdc), as shown previ-

ously via breakthrough experiments under dry and wet conditions.<sup>15</sup> Our findings are fully consistent with the known instability of carbamic acid under wet conditions in other materials,<sup>35,40</sup> as well as the stabilization of ammonium carbamates by hydrogen-bonding interactions with water.<sup>24</sup>

## CONCLUSIONS

We have carried out a systematic study of CO<sub>2</sub> chemisorption in materials of the type diamine–M<sub>2</sub>(dobpdc). The canonical chemisorption products of ammonium carbamate chains and carbamic acid pairs have been thoroughly characterized using multinuclear NMR experiments and vdW-corrected DFT calculations. Our results demonstrate the importance of using multiple experimental and calculated NMR parameters to make accurate structural assignments. In particular, <sup>13</sup>C NMR experiments and calculations alone may be insufficient to make accurate structural assignments, owing to the small range of <sup>13</sup>C chemical shifts for the possible chemisorption products and relatively large discrepancies between experimental and calculated shift values. Nonetheless, the ranges determined here for chemical shift parameters of different chemisorption products can guide structural assignments following CO<sub>2</sub> adsorption in the wider family of amine-functionalized materials (Figure 6). Ultimately, experiments and calculations that give information on the connectivity of the various groups (such as <sup>1</sup>H–<sup>13</sup>C two dimensional HETCOR experiments) can enable clearer assignments of carbamic acid and ammonium carbamate groups.

Our results also indicate that ammonium carbamate chain formation dominates for a wide range of diamine–Mg<sub>2</sub>(dobpdc) materials, with the exclusive formation of carbamic acid pairs only observed thus far for dmpn–Zn<sub>2</sub>(dobpdc). Furthermore, we have demonstrated that a new mixed chemisorption mechanism can occur, wherein ammonium carbamate and carbamic acid form in a 1:1 ratio. Using a combination of NMR spectroscopy and DFT calculations, we have proposed a structure for the mixed chemisorption product in dmpn–Mg<sub>2</sub>(dobpdc), whereby both ammonium carbamate and carbamic acid chains form along the *c* axis while interacting across the framework pore. This new mechanism accounts for the unusual adsorption properties of this material and helps to explain its excellent performance for CO<sub>2</sub> capture from coal flue gas. The further development of amine-appended adsorbents with bulky functional groups therefore offers an important route for tuning the chemisorption of CO<sub>2</sub> and the thermodynamics for CO<sub>2</sub> capture at different partial pressures. Finally, our results highlight the importance of water in directing CO<sub>2</sub> chemisorption in diamine-appended MOFs, supporting the conclusions of previous studies that ammonium carbamate formation is favored and carbamic acid formation is disfavored in the presence of water.<sup>35,40</sup> The rich chemistry of amine-functionalized materials will undoubtedly continue to reveal more complexity as increasingly diverse materials are explored. We anticipate that understanding and controlling this complexity will enable the design of improved materials for CO<sub>2</sub> capture.

## EXPERIMENTAL

**Materials.** Diamines and solvents were purchased from commercial sources and used as received. The ligand H<sub>4</sub>dobpdc was purchased from Hangzhou Trylead Chemical Technology Co and used as received.

**Synthesis of Mg<sub>2</sub>(dobpdc).** The framework was prepared according to the literature procedure.<sup>14</sup> An Erlenmeyer flask was charged with Mg(NO<sub>3</sub>)<sub>2</sub>·6H<sub>2</sub>O (11.5 g, 45.0 mmol, 1.24 equiv), 4,4'-dihydroxy-[1,1'-

biphenyl]-3,3'-dicarboxylic acid (9.90 g, 36.0 mmol, 1.00 equiv), *N,N*-dimethylformamide (90 mL), and methanol (110 mL). The mixture was sonicated until the solids dissolved and was then filtered through filter paper into a 350 mL screw-cap high-pressure reaction vessel equipped with a stir bar. The reaction mixture was sparged with N<sub>2</sub> for 1 h, and then the reaction vessel was sealed and the reaction mixture stirred slowly at 120 °C for 14 h, resulting in precipitation of a white solid from solution. The mixture was filtered to collect the solid, and the solid was quickly transferred to a Pyrex jar filled with *N,N*-dimethylformamide (500 mL). This was placed in an oven heated to 60 °C and allowed to stand for at least 3 h. At this time, the mixture was filtered and the solid was returned to the jar with fresh *N,N*-dimethylformamide (500 mL) and placed in an oven heated to 60 °C for a further 3 h. This washing process was repeated a total of three times. The *N,N*-dimethylformamide was replaced with methanol (500 mL), and this washing process was repeated a further three times with methanol. A small portion of the solid was then removed and placed in a vial under flowing N<sub>2</sub>. The remaining solid was activated under flowing N<sub>2</sub> at 180 °C for 24 h, transferred to a glass adsorption tube equipped with a Micromeritics TransSeal, and activated for an additional 24 h under reduced pressure (<10 μbar) at 180 °C. Activated Mg<sub>2</sub>(dobpdc) was obtained as a white solid. Langmuir surface area determined from the 77 K N<sub>2</sub> adsorption isotherm: 3900 m<sup>2</sup>/g.

**Synthesis of Zn<sub>2</sub>(dobpdc).** An Erlenmeyer flask was charged with Zn(NO<sub>3</sub>)<sub>2</sub>·6H<sub>2</sub>O (3.72 g, 12.5 mmol, 2.50 equiv), 4,4'-dihydroxy-[1,1'-biphenyl]-3,3'-dicarboxylic acid (1.37 g, 5.00 mmol, 1.00 equiv), *N,N*-dimethylformamide (250 mL), and methanol (250 mL). The mixture was sonicated until the solids dissolved and filtered through filter paper into a 1 L Pyrex jar. The reaction mixture was vigorously sparged with N<sub>2</sub> for 1 h, and the jar was placed in an oven at 120 °C and allowed to stand for 14 h, resulting in precipitation of an off-white solid from solution. The non-homogenous mixture was filtered to collect the solid, and the solid was quickly transferred to a Pyrex jar filled with *N,N*-dimethylformamide (500 mL). The jar was placed in an oven heated to 60 °C and allowed to stand for at least 3 h. At this time, the mixture was filtered and the solid was returned to the jar with fresh *N,N*-dimethylformamide (500 mL) and placed again in an oven heated to 60 °C for 3 h. This washing process was repeated a total of three times. The *N,N*-dimethylformamide was replaced with methanol (500 mL), and this washing process was repeated a further three times with methanol. The mixture was filtered, and the collected solid was transferred to a Schlenk flask and activated under flowing N<sub>2</sub> at 180 °C for 8 h followed by heating under high vacuum at 180 °C for 24 h. The Schlenk flask was transferred into a N<sub>2</sub>-filled glovebox, and the solid was transferred to a glass adsorption tube equipped with a Micromeritics TransSeal and activated for an additional 24 h under high vacuum (<10 μbar) at 180 °C. Activated Zn<sub>2</sub>(dobpdc) was obtained as 1.89 g (94%) of an off-white solid. Langmuir surface area determined from the 77 K N<sub>2</sub> adsorption isotherm: 3130 m<sup>2</sup>/g. Note: methanol-solvated Zn<sub>2</sub>(dobpdc) slowly degrades in the presence of air and thus should be stored activated in a N<sub>2</sub>-filled glovebox when not in use.

**Synthesis of H<sub>4</sub>(dotpdc).** The ligand was prepared according to the literature procedure.<sup>54</sup> A 500 mL roundbottom flask was charged with a Teflon-coated magnetic stir bar, K<sub>2</sub>CO<sub>3</sub> (31.1 g, 225 mmol, 3.00 equiv), and 5-bromosalicylic acid (9.80 g, 45.0 mmol, 1.00 equiv). *N,N*-dimethylformamide (250 mL) was added, and the flask was placed in an ice water bath. Iodomethane (8.40 g, 135 mmol, 3.00 equiv) was added slowly (~1 drop/s), and the reaction mixture was stirred vigorously at room temperature for 20 h. The reaction mixture was then poured into 1.5 L of ice water and vigorously stirred for 10 min. The resulting mixture was filtered to yield 5-bromo-2-methoxybenzoate (7.28 g, 65.7% yield). <sup>1</sup>H NMR (in CDCl<sub>3</sub> solvent) was consistent with that reported in the literature.<sup>54</sup> δ 7.84 (d, *J* = 3 Hz, 1H), 7.50 (dd, *J* = 9, 3 Hz, 1H), 6.80 (d, *J* = 9 Hz, 1H), 3.83 (s, 3H), 3.81 (s, 3H) ppm.

A 50 mL 3-neck roundbottom flask equipped with a Teflon-coated magnetic stir bar and a reflux condenser was charged with 5-bromo-2-methoxybenzoate (3.60 g, 14.7 mmol, 2.20 equiv), XPhos Pd G2 (0.234 g, 0.30 mmol, 0.05 equiv), and benzene-1,4-diboric acid (0.234 g, 0.30 mmol, 0.05 equiv). The flask was placed under vacuum for 5 min, and

then back-filled with nitrogen. This process was repeated a total of 3 times. Next, degassed tetrahydrofuran (8 mL) and  $\text{K}_2\text{CO}_3$  (8.11 g, 58.7 mmol, 4 equiv, dissolved in water at 0.5 M) were added via syringe and the reaction mixture was allowed to stir under reflux for 20 h, during which time a gray solid precipitated from solution. The reaction mixture was cooled to room temperature and then poured into 75 mL of cold water. The mixture was then filtered, and the precipitate washed with  $3 \times 10$  mL cold water. The gray solid was dissolved in 100 mL hot  $\text{CH}_2\text{Cl}_2$  and then filtered through celite and eluted with an additional 300 mL  $\text{CH}_2\text{Cl}_2$ . The resulting brown solid was then concentrated *in vacuo*. The solid was triturated with 20 mL cold methanol, then filtered and washed with  $2 \times 5$  mL cold methanol. This trituration and filtration step was repeated two times to yield off-white dimethyl 4,4''-dimethoxy-[1,1':4',1''-terphenyl]-3,3''-dicarboxylate (2.32 g, 96.4% yield).  $^1\text{H}$  NMR (in  $\text{CDCl}_3$  solvent) was consistent with that reported in the literature.<sup>54</sup>  $\delta$  8.07 (d,  $J = 2$  Hz, 2H), 7.72 (dd,  $J = 9, 2$  Hz, 2H), 7.61 (s, 4H), 7.05 (d,  $J = 9$  Hz, 2H), 3.94 (s, 6H), 3.91 (s, 6H) ppm.

A 100 mL roundbottom flask was equipped with a stir bar and reflux condenser and charged with dimethyl 4,4''-dimethoxy-[1,1':4',1''-terphenyl]-3,3''-dicarboxylate (2.21 g, 5.40 mmol, 1.00 equiv). HBr and AcOH (90 mL each) were added to the flask, and the solution was allowed to reflux for 24 h. During this time, the mixture turned orange, and a white solid precipitated from solution. The reaction was allowed to cool to room temperature, then poured into 200 mL cold water and filtered. By NMR spectroscopy, a 7% impurity of the starting material was found, so the sample was refluxed under the same conditions and acid amounts for an additional 48 h. It was then washed with  $2 \times 50$  mL cold water to yield  $\text{H}_4(\text{dotpdc})$  (4,4''-dihydroxy-[1,1':4',1''-terphenyl]-3,3''-dicarboxylic acid) (96.0% yield).  $^1\text{H}$  NMR (in  $\text{DMSO}-d_6$ ) was consistent with that reported in the literature.<sup>54</sup>  $\delta$  14.1 (bs, 2H), 11.2 (bs, 2H), 8.07 (s, 2H), 7.86 (d,  $J = 9$  Hz, 2H), 7.71 (s, 4H), 7.07 (d,  $J = 9$  Hz, 2H) ppm.

**Synthesis of  $\text{Mg}_2(\text{dotpdc})$ :** A synthetic route very similar to that previously reported<sup>54</sup> was followed. A 20 mL scintillation vial was charged with  $\text{H}_4(\text{dotpdc})$  (4,4''-dihydroxy-[1,1':4',1''-terphenyl]-3,3''-dicarboxylic acid) (35.0 mg, 0.103 mmol, 1.00 equiv) and  $\text{Mg}(\text{NO}_3)_2 \cdot 6\text{H}_2\text{O}$  (64.0 mg, 0.250 mmol, 2.50 equiv). Methanol (5.5 mL) and fresh  $N,N$ -dimethylformamide (4.5 mL) were added to the vial, and the solution was sonicated until all of the solids dissolved. The threads of the vial were wrapped in Teflon tape, sealed with a Teflon lined cap, and heated at 120 °C in a heating block for 14 h, during which time a white solid precipitated from solution. The vial was cooled to room temperature and the mixture filtered to collect the solid, which was washed thoroughly with fresh  $N,N$ -dimethylformamide (15 mL). The solid was then transferred to a vial filled with fresh  $N,N$ -dimethylformamide (10 mL) and allowed to soak at 60 °C for at least 3 h. The supernatant was decanted and replaced with fresh  $N,N$ -dimethylformamide (10 mL). This process was repeated a total of three times. The  $N,N$ -dimethylformamide was replaced with methanol (10 mL), and the off-white solid was soaked in methanol at 60 °C for at least 3 h. The supernatant was decanted and replaced with fresh methanol (10 mL). This process was repeated a total of three times to obtain the final  $\text{Mg}_2(\text{dotpdc})$  product as a pale yellow solid. Langmuir surface area determined from the 77 K  $\text{N}_2$  adsorption isotherm: 5770  $\text{m}^2/\text{g}$ .

**Synthesis of Diamine-Appended Metal–Organic Frameworks.** Diamine-appended metal–organic frameworks were synthesized by directly grafting diamines to methanol-solvated  $\text{M}_2(\text{dobpdc})$  materials, as previously reported.<sup>14</sup> First, methanol-solvated materials ( $\text{Mg}_2(\text{dobpdc})$ ,  $\text{Zn}_2(\text{dobpdc})$ , or  $\text{Mg}_2(\text{dotpdc})$ ) were filtered and washed with toluene (~50 mL). The filtered framework was then added to 5 mL of a 20% (v/v) solution of diamine in toluene. After soaking for at least 12 h, the solid was obtained by filtration and washed with toluene (~50 mL) to remove excess diamine before proceeding to activation. Note: for the preparation of e-2- $\text{Mg}_2(\text{dobpdc})$ , waiting for 0.5 h was sufficient for complete diamine-appending, although this faster route has not yet been explored for other materials.

For e-2- $\text{Zn}_2(\text{dobpdc})$  a different method was used. Under  $\text{N}_2$ , a 30 mL scintillation vial was charged with freshly-filtered methanol-solvated  $\text{Zn}_2(\text{dobpdc})$  (~20 mg), and the vial was heated at 180 °C for 24 h under

flowing  $\text{N}_2$ . Meanwhile, freshly-ground  $\text{CaH}_2$  (~30 mg) was added to a solution of 1 mL of e-2 and 4 mL of toluene in a 30 mL scintillation vial equipped with a stir bar. The mixture was stirred at 100 °C under flowing  $\text{N}_2$  for 30 min and then allowed to cool to room temperature and settle overnight. The dried diamine solution and activated  $\text{Zn}_2(\text{dobpdc})$  were transferred to a  $\text{N}_2$ -filled glovebag, and the diamine solution was carefully decanted from the  $\text{CaH}_2$  and added via syringe to the  $\text{Zn}_2(\text{dobpdc})$  sample. The vial containing the framework and diamine was then swirled several times and allowed to stand at room temperature for 0.5 h. At this time, the mixture was filtered, and the resulting powder was thoroughly washed with successive aliquots of toluene ( $3 \times 20$  mL) and allowed to dry on the filter paper for several minutes before proceeding to activation.

All diamine-appended MOF samples were activated under flowing  $\text{N}_2$  using activation times and heating temperatures specified in Table S3 in the Supporting Information. Diamine loadings were determined by quantitative  $^1\text{H}$  NMR experiments of digested frameworks and were  $100 \pm 5\%$  for the majority of the studied materials (Table S3). For digestion, ~5 mg of diamine appended framework was added to a mixture consisting of 1 mL of  $\text{DMSO}-d_6$  and two Pasteur pipette drops of DCl solution (35 wt. % in  $\text{D}_2\text{O}$ ,  $\geq 99$  atom % D).

**NMR Sample Preparation.** Activated diamine-appended framework samples were packed into 3.2 mm rotors inside a nitrogen-filled glove bag. Each sample was then evacuated inside a home-built gas manifold (Figure 2) for at least 10 min. The key feature of this gas dosing manifold is that rotors may be dosed at different gas pressures, then closed while still inside the manifold.<sup>15</sup> Samples were dosed with  $^{13}\text{CO}_2$  gas (Sigma-Aldrich, 99 atom %  $^{13}\text{C}$ , < 3 atom %  $^{18}\text{O}$ ) and allowed to equilibrate for at least 30 min (unless otherwise stated). Gas pressures (see Figure captions) were recorded immediately before closing the rotor inside the home-built gas manifold. Gas dosing was carried out at room temperature (24(2) °C).  $^{13}\text{C}$  NMR experiments as a function of time indicated minimal changes to the chemisorbed  $\text{CO}_2$  resonance during the time needed for acquisition of NMR data (Figure S23). An exception to this is experiments on  $\text{dmpn}-\text{Zn}_2(\text{dobpdc})$  dosed at 1 bar  $^{13}\text{CO}_2$ , where small losses of  $\text{CO}_2$  from the rotor led to a transition from the carbamic acid pair structure to the mixed chemisorption structure on a timescale of ~10 hours. Here experiment times thus had to be limited to avoid structural changes during the NMR experiment (this accounts for the low signal to noise ratio in the bottom spectrum in Figure 4c).

For experiments under wet conditions, each activated diamine- $\text{Mg}_2(\text{dobpdc})$  sample was initially characterized with NMR spectroscopy and the sample was then exposed to wet  $\text{N}_2$  (generated by flowing  $\text{N}_2$  gas through a bubbler containing deionized water) for 30 min, and further NMR spectra were recorded. The sample was then inserted into the home-built gas-dosing manifold, evacuated for 10 min, and then dosed with dry  $^{13}\text{CO}_2$  before recording additional NMR spectra. Dosing times were 30 min for e-2- $\text{Mg}_2(\text{dobpdc})$  and 15 h for  $\text{dmpn}-\text{Mg}_2(\text{dobpdc})$ . Additional data was collected on initially activated framework samples that were then first dosed with dry  $^{13}\text{CO}_2$  before exposure to wet natural abundance  $\text{CO}_2$  gas (99.998% Praxair, research grade), see Figure S21.

**NMR Experiments.** All NMR experiments were carried out at 16.4 T using a Bruker 3.2 mm magic angle spinning (MAS) probe with a MAS rate of 15 kHz in all cases. Carbon-13 NMR spectra were in general acquired by cross-polarization from  $^1\text{H}$ , though direct polarization was used for the spectrum in Figure 3a. For quantification of  $^{13}\text{C}$  resonances, direct excitation experiments were used with continuous wave decoupling and with sufficiently long recycle delays to yield quantitative data. Dmfit software<sup>55</sup> was used to fit the spectra and quantify the proportions of the different  $^{13}\text{C}$  resonances. Nitrogen-15 NMR spectra were acquired by cross-polarization from  $^1\text{H}$ . All cross-polarization experiments were acquired with continuous wave  $^1\text{H}$  decoupling at ~80 kHz radio frequency field strength and with contact times of either 100  $\mu\text{s}$  or 1 ms as specified in the figure captions. For two-dimensional experiments, a HETCOR experiment employing cross-polarization from  $^1\text{H}$  to  $^{13}\text{C}$  was used according to the sequence:  $90^\circ(^1\text{H}) - t_1 - \text{cross-polarization} - t_2$ , again using continuous wave  $^1\text{H}$  decoupling. Proton NMR spectra were acquired using a  $90^\circ$  pulse-acquire sequence. Proton,  $^{13}\text{C}$ , and  $^{15}\text{N}$  chemical shifts were referenced to 1.8 ppm (adamantane), 38.5 ppm (adamantane,



tertiary carbon – left hand resonance), and 33.4 ppm (glycine),<sup>56</sup> respectively. NMR experiments were performed at room temperature without temperature control. The temperature increase due to frictional heating at 15 kHz MAS in a 3.2 mm is expected to be approximately 12 K.<sup>57</sup>

**Computational Details.** In order to elucidate the local structures of the various diamine-appended frameworks, we performed first-principles density functional theory (DFT) calculations. We used a plane-wave basis and projector augmented-wave (PAW)<sup>58,59</sup> pseudopotentials with the Vienna *ab initio* Simulation Package (VASP) code.<sup>60–63</sup> To include the effect of the van der Waals (vdW) dispersive interactions on binding energies, we performed structural relaxations with vdW dispersion-corrected functionals (vdW-DF2)<sup>64</sup> as implemented in VASP. DFT binding energies were calculated using  $\Delta E_{\text{ads}} = E_{(\text{CO}_2)\text{-diamine-M}_2(\text{dobpdc})} - (E_{(\text{diamine-M}_2(\text{dobpdc}))} + E_{\text{CO}_2})$ , where the contributions of the zero-point energy and thermal energy corrections are neglected, as these are generally less than 2 kJ/mol.<sup>24</sup> For these CO<sub>2</sub> binding energy calculations, we used (i) a  $\Gamma$ -point sampling of the Brillouin zone and (ii) a 600 eV plane-wave cutoff energy. We explicitly treated two valence electrons for Mg (3s<sup>2</sup>), twelve for Zn (3d<sup>10</sup>4s<sup>2</sup>), six for O (2s<sup>2</sup>2p<sup>4</sup>), five for N (2s<sup>2</sup>2p<sup>3</sup>), four for C (2s<sup>2</sup>2p<sup>2</sup>), and one for H(1s<sup>1</sup>). All structural relaxations were performed with a Gaussian smearing of the electronic occupations of 0.05 eV.<sup>65</sup> The ions were relaxed until the Hellmann-Feynman forces were less than 0.02 eV Å<sup>-1</sup>. The convergence threshold for self-consistency in the total energy was 10<sup>-5</sup> eV.

For NMR chemical shift calculations, we performed structural relaxations with (i) a 1000 eV plane-wave cutoff energy, (ii) a 0.01 eV Å<sup>-1</sup> force criterion, (iii) a 1 × 1 × 3 k-point grid, (iv) a 10<sup>-7</sup> eV self-consistency criterion, and (v) the PBE functional<sup>66</sup> with the D3 vdW correction;<sup>67,68</sup> see Table S4 for optimized lattice parameters. In these input criteria, the isotropic chemical shielding ( $\sigma_{\text{iso}}$ ) converged within 0.1 ppm. The isotropic chemical shift ( $\delta_{\text{iso}}$ ) was obtained using  $\delta_{\text{iso}} = -(\sigma_{\text{iso}} - \sigma_{\text{ref}})$ , where  $\sigma_{\text{ref}}$  is a reference shielding value that is 30.9 ppm, 170.5 ppm, and 225.0 ppm for <sup>1</sup>H, <sup>13</sup>C and <sup>15</sup>N, respectively. The  $\sigma_{\text{ref}}$  values for <sup>1</sup>H and <sup>13</sup>C were obtained by first computing  $\sigma_{\text{iso}}$  values for cocaine (CSD entry code: COCAIN10 was used as the starting point and the structure was geometry optimized before NMR calculation). Cocaine was used for shift referencing as it has several <sup>1</sup>H and <sup>13</sup>C resonances for comparison between experiment and calculation. DFT-calculated values were compared to published experimental values,<sup>69</sup> with  $\sigma_{\text{ref}}$  given as the y-intercept of a linear fit (with a fixed gradient of -1) in a plot of  $\delta_{\text{iso}}$  (experimental) vs.  $\sigma_{\text{iso}}$  (calculated). The  $\sigma_{\text{ref}}$  value for <sup>15</sup>N was determined by comparison of DFT-calculated  $\sigma_{\text{iso}}$  and the experimental  $\delta_{\text{iso}}$  value for glycine.

**Gas Adsorption.** The CO<sub>2</sub> adsorption isotherm for e-2-Mg<sub>2</sub>(dobpdc) was obtained by a volumetric method using a Micromeritics 3Flex gas adsorption analyzer and research-grade (> 99.998%) CO<sub>2</sub> and He. Approximately 80 mg of the framework was loaded into a pre-weighed sample tube, which was first transferred to a Micromeritics 2420 degas manifold and heated to 100 °C at a rate of 5 °C/min under reduced pressure (< 10 μbar). The sample was held under vacuum at 100 °C for ~3 h, after which the evacuated tube was weighed to determine the mass of the degassed sample. The sample was then transferred air-free to the analysis port of the 3Flex adsorption analyzer and immersed in a temperature-controlled oil bath at 26(1) °C. Equilibration was defined as < 0.01% change in average pressure over an equilibration interval of 30 s. Gas adsorption isotherm data for dmpn-Mg<sub>2</sub>(dobpdc) and dmpn-Zn<sub>2</sub>(dobpdc) at 25 °C was taken directly from a previous study.<sup>15</sup>

Thermogravimetric analysis (TGA) experiments were conducted using a TA Instruments TGA Q5000. Isobars were measured using a temperature ramp rate of 1 °C/min, except where otherwise indicated. Samples were first activated at 130 or 150 °C (for dmpn-Mg<sub>2</sub>(dobpdc) and Mg<sub>2</sub>(dotpdc), respectively) under flowing N<sub>2</sub> for 20 min prior to switching the gas stream to CO<sub>2</sub> and cooling. Masses are uncorrected for buoyancy effects.

## ASSOCIATED CONTENT

### Supporting Information

The Supporting Information is available free of charge on the ACS Publications website.

Gas adsorption data, NMR spectra, powder X-ray diffraction patterns and discussion, sample activation conditions and diamine loadings. (PDF)

Structure files generated by DFT calculations with the PBE functional and the D3 vdW correction (CIF).

## AUTHOR INFORMATION

### Corresponding Authors

\*reimer@berkeley.edu

\*jrlong@berkeley.edu

\*jbneaton@berkeley.edu

### Present Addresses

†P.J.M. Department of Chemistry and Chemical Biology, Cornell University, Ithaca, NY, 14853, U.S.A.

## ACKNOWLEDGEMENTS

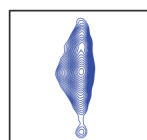
The experiments investigating dmpn-Mg<sub>2</sub>(dobpdc) and all of the computational studies were supported by the U.S. Department of Energy (DOE) under NETL grant FWP-00006194. All other experimental work was supported through the Center for Gas Separations Relevant to Clean Energy Technologies, an Energy Frontier Research Center funded by the U.S. Department of Energy (DOE), Office of Science, Office of Basic Energy Sciences, under Award DE-SC0001015. We note that the original syntheses and initial characterization of dmpn-Mg<sub>2</sub>(dobpdc), mpn-Mg<sub>2</sub>(dobpdc), pn-Mg<sub>2</sub>(dobpdc), Mg<sub>2</sub>(dotpdc), and nPr-2-Mg<sub>2</sub>(dotpdc), as reported previously in Refs. 15 and 16, was supported by ExxonMobil Research and Engineering Company. Work at the Molecular Foundry was further supported by the Office of Science, Office of Basic Energy Sciences, U.S. Department of Energy, under Contract DE-AC02-05CH11231, and computational resources were provided by DOE (LBNL Lawrence Livermore and NERSC). This research also used the Savio computational cluster resource provided by the Berkeley Research Computing program at the University of California, Berkeley (supported by the UC Berkeley Chancellor, Vice Chancellor for Research, and Chief Information Officer). Use of the Advanced Photon Source at Argonne National Laboratory was supported by the U. S. Department of Energy, Office of Science, Office of Basic Energy Sciences, under Contract No. DE-AC02-06CH11357. We thank the Philomathia Foundation and Berkeley Energy and Climate Institute for support of A.C.F. through a postdoctoral fellowship, the National Institutes of Health for support of P.J.M. through a postdoctoral fellowship (GM120799), and the Miller Institute for Basic Research in Science for support of J.D.M. through a postdoctoral fellowship. The content is solely the responsibility of the authors and does not necessarily represent the official views of the National Institutes of Health. We further thank Dr. Richard Bounds and Thomas M. Osborn Popp for assistance with the development of gas dosing equipment for NMR experiments and useful discussions. Maria Paley is thanked for assistance with powder X-ray diffraction measurements, Dr. Jun Xu is thanked for useful discussions, and Dr. Katie R. Meihuis is thanked for editorial assistance.

## REFERENCES

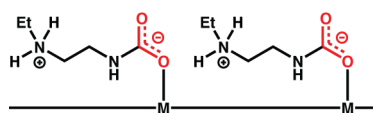
- (1) IPCC, 2014: Climate Change 2014: Synthesis Report. Contribution of Working Groups I, II and III to the Fifth Assessment Report of the Intergovernmental Panel on Climate Change [Core Writing Team, R.K. Pachauri and L.A. Meyer (Eds.)]. IPCC, Geneva, Switzerland. 2014.

- (2) Bourzac, K. We Have the Technology. *Nature* **2017**, *550*, S66–S69.
- (3) Choi, S.; Drese, J. H.; Jones, C. W. Adsorbent Materials for Carbon Dioxide Capture from Large Anthropogenic Point Sources. *Chem. Sus. Chem.* **2009**, *2*, 796–854.
- (4) McDonald, T. M.; Lee, W. R.; Mason, J. A.; Wiers, B. M.; Hong, C. S.; Long, J. R. Capture of Carbon Dioxide from Air and Flue Gas in the Alkylamine-Appended Metal–Organic Framework Mmen-Mg<sub>2</sub>(dobpdc). *J. Am. Chem. Soc.* **2012**, *134*, 7056–7065.
- (5) McDonald, T. M.; Mason, J. A.; Kong, X.; Bloch, E. D.; Gygi, D.; Dani, A.; Crocellà, V.; Giordanino, F.; Odoh, S. O.; Drisdell, W. S.; et al. Cooperative Insertion of CO<sub>2</sub> in Diamine-Appended Metal–Organic Frameworks. *Nature* **2015**, *519*, 303–308.
- (6) McDonald, T. M.; D'Alessandro, D. M.; Krishna, R.; Long, J. R. Enhanced Carbon Dioxide Capture upon Incorporation of N,N'-Dimethylethylenediamine in the Metal–Organic Framework Cu<sup>II</sup>BTTC. *Chem. Sci.* **2011**, *2*, 2022.
- (7) Lin, Y.; Kong, C.; Chen, L. Amine-Functionalized Metal–Organic Frameworks: Structure, Synthesis and Applications. *RSC Adv.* **2016**, *6*, 32598–32614.
- (8) Bernini, M. C.; Blanco, A. A. G.; Villarroel-Rocha, J.; Fairen-Jimenez, D.; Sapag, K.; Ramirez-Pastor, A. J.; Narda, G. E. Tuning the Target Composition of Amine-Grafted CPO-27-Mg for Capture of CO<sub>2</sub> under Post-Combustion and Air Filtering Conditions: A Combined Experimental and Computational Study. *Dalt. Trans.* **2015**, *44*, 18970–18982.
- (9) Yeon, J. S.; Lee, W. R.; Kim, N. W.; Jo, H.; Lee, H.; Song, J. H.; Lim, K. S.; Kang, D. W.; Seo, J. G.; Moon, D.; et al. Homodiamine-Functionalized Metal–Organic Frameworks with a MOF-74-Type Extended Structure for Superior Selectivity of CO<sub>2</sub> over N<sub>2</sub>. *J. Mater. Chem. A* **2015**, *3*, 19177–19185.
- (10) Hu, Y.; Verdegaa, W. M.; Yu, S.; Jiang, H.-L. Alkylamine-Tethered Stable Metal–Organic Framework for CO<sub>2</sub> Capture from Flue Gas. *Chem. Sus. Chem.* **2014**, *7*, 734–737.
- (11) Demessence, A.; Alessandri, D. M. D.; Foo, M. L.; Long, J. R. Strong CO<sub>2</sub> Binding in a Water-Stable, Triazolate-Bridged Metal–Organic Framework Functionalized with Ethylenediamine. *J. Am. Chem. Soc.* **2009**, *131*, 8784–8786.
- (12) Choi, S.; Watanabe, T.; Bae, T.; Sholl, D. S.; Jones, C. W. Modification of the Mg/DOBDC MOF with Amines to Enhance CO<sub>2</sub> Adsorption from Ultradilute Gases. *J. Phys. Chem. C* **2012**, *116*, 1136–1141.
- (13) Fracaroli, A. M.; Furukawa, H.; Suzuki, M.; Dodd, M.; Okajima, S.; Gandara, F.; Reimer, J. A.; Yaghi, O. M. Metal–Organic Frameworks with Precisely Designed Interior for Carbon Dioxide Capture in the Presence of Water. *J. Am. Chem. Soc.* **2014**, *136*, 8863–8866.
- (14) Siegelman, R. L.; McDonald, T. M.; Gonzalez, M. I.; Martell, J. D.; Milner, P. J.; Mason, J. A.; Berger, A. H.; Bhowan, A. S.; Long, J. R. Controlling Cooperative CO<sub>2</sub> Adsorption in Diamine-Appended Mg<sub>2</sub>(dobpdc) Metal–Organic Frameworks. *J. Am. Chem. Soc.* **2017**, *139*, 10526–10538.
- (15) Milner, P. J.; Siegelman, R. L.; Forse, A. C.; Gonzalez, M. I.; Runčevski, T.; Martell, J. D.; Reimer, J. A.; Long, J. R. A Diaminopropane-Appended Metal–Organic Framework Enabling Efficient CO<sub>2</sub> Capture from Coal Flue Gas via a Mixed Adsorption Mechanism. *J. Am. Chem. Soc.* **2017**, *139*, 13541–13553.
- (16) Milner, P. J.; Martell, J. D.; Siegelman, R. L.; Gygi, D.; Weston, S. C.; Long, J. R. Overcoming Double-Step CO<sub>2</sub> Adsorption and Minimizing Water Co-Adsorption in Bulky Diamine-Appended Variants of Mg<sub>2</sub>(dobpdc). *Chem. Sci.* **2018**, *9*, 160–174.
- (17) Lee, W. R.; Jo, H.; Yang, L.-M.; Lee, H.; Ryu, D. W.; Lim, K. S.; Song, J. H.; Min, D. Y.; Han, S. S.; Seo, J. G.; et al. Exceptional CO<sub>2</sub> Working Capacity in a Heterodiamine-Grafted Metal–Organic Framework. *Chem. Sci.* **2015**, *6*, 3697–3705.
- (18) Jo, H.; Lee, W. R.; Kim, N. W.; Jung, H.; Lim, K. S.; Kim, J. E.; Kang, D. W.; Lee, H.; Hiremath, V.; Seo, J. G.; et al. Fine-Tuning of the Carbon Dioxide Capture Capability of Diamine-Grafted Metal–Organic Framework Adsorbents Through Amine Functionalization. *Chem. Sus. Chem.* **2017**, *2*, 541–550.
- (19) Martell, J. D.; Porter-Zasada, L. B.; Forse, A. C.; Siegelman, R. L.; Gonzalez, M. I.; Oktawiec, J.; Xu, J.; Srebro-Hooper, M.; Milner, P. J.; Colwell, K. A.; et al. Enantioselective Recognition of Ammonium Carbamates in a Chiral Metal–Organic Framework. *J. Am. Chem. Soc.* **2017**, *139*, 16000–16012.
- (20) Vlaisavljevich, B.; Odoh, S. O.; Schnell, S. K.; Dzubak, A. L.; Lee, K.; Planas, N.; Neaton, J. B.; Gagliardi, L.; Smit, B. CO<sub>2</sub> Induced Phase Transitions in Diamine-Appended Metal–Organic Frameworks. *Chem. Sci.* **2015**, *6*, 5177–5185.
- (21) Hefti, M.; Joss, L.; Bjelobrk, Z.; Mazzotti, M. On the Potential of Phase-Change Adsorbents for CO<sub>2</sub> Capture by Temperature Swing Adsorption. *Faraday Discuss.* **2016**, *192*, 153–179.
- (22) Joss, L.; Hefti, M.; Bjelobrk, Z.; Mazzotti, M. On the Potential of Phase-Change Adsorbents for CO<sub>2</sub> Capture by Temperature Swing Adsorption. *Energy Procedia* **2017**, *114*, 2271–2278.
- (23) Sinha, A.; Darunte, L. A.; Jones, C. W.; Realf, M. J.; Kawajiri, Y. Systems Design and Economic Analysis of Direct Air Capture of CO<sub>2</sub> through Temperature Vacuum Swing Adsorption Using MIL-101(Cr)-PEI-800 and Mmen-Mg<sub>2</sub>(dobpdc) MOF Adsorbents. *Ind. Eng. Chem. Res.* **2017**, *56*, 750–764.
- (24) Lee, J.-H.; Siegelman, R. L.; Maserati, L.; Rangel, T.; Helms, B. A.; Long, J. R.; Neaton, J. B. Enhancement of CO<sub>2</sub> Binding and Mechanical Properties upon Diamine Functionalization of M<sub>2</sub>(dobpdc) Metal–Organic Frameworks. *Chem. Sci.* **2018**, *2*, DOI:10.1039/c7sc05217k.
- (25) Drisdell, W. S.; Poloni, R.; McDonald, T. M.; Pascal, T. A.; Wan, L. F.; Pemmaraju, C. Das; Vlaisavljevich, B.; Odoh, S. O.; Neaton, J. B.; Long, J. R.; et al. Probing the Mechanism of CO<sub>2</sub> Capture in Diamine-Appended Metal–Organic Frameworks Using Measured and Simulated X-Ray Spectroscopy. *Phys. Chem. Chem. Phys.* **2015**, *17*, 21448–21457.
- (26) Kundu, J.; Stilck, J. F.; Lee, J.-H.; Neaton, J. B.; Prendergast, D.; Whitelam, S. Cooperative Gas Adsorption without a Phase Transition in Metal–Organic Frameworks. *Phys. Rev. Lett.* **2018**, *121*, 15701.
- (27) Pramchu, S.; Jaroenjitichai, A. P.; Laosiritaworn, Y. Tuning Carbon Dioxide Capture Capability with Structural and Compositional Design in Mmen-(Mg,Zn) (Dobpdc) Metal–Organic Framework: Density Functional Theory Investigation. *Greenh. Gas Sci Technol.* **2018**, DOI:10.1002/ghg.1768.
- (28) Forse, A. C.; Gonzalez, M. I.; Siegelman, R. L.; Witherspoon, V. J.; Jawahery, S.; Mercado, R.; Milner, P. J.; Martell, J. D.; Smit, B.; Blümich, B.; et al. Unexpected Diffusion Anisotropy of Carbon Dioxide in the Metal–Organic Framework Zn<sub>2</sub>(dobpdc). *J. Am. Chem. Soc.* **2018**, *140*, 1663–1673.
- (29) Planas, N.; Dzubak, A. L.; Poloni, R.; Lin, L.; Mcmanus, A.; McDonald, T. M.; Neaton, J. B.; Long, R.; Smit, B.; Gagliardi, L. The Mechanism of Carbon Dioxide Adsorption in an Alkylamine-Functionalized Metal–Organic Framework. *J. Am. Chem. Soc.* **2013**, *135*, 10–13.
- (30) Tsuda, T.; Fujiwara, T. Polyethyleneimine and Macrocyclic Polyamine Silica Gels Acting as Carbon Dioxide Absorbents. *J. Chem. Soc. Chem. Commun.* **1992**, *1*, 1659–1661.
- (31) Xu, X.; Song, C.; Andresen, J. M.; Miller, B. G.; Scaroni, A. W. Novel Polyethyleneimine-Modified Mesoporous Molecular Sieve of MCM-41 Type as High-Capacity Adsorbent for CO<sub>2</sub> Capture. *Energy & Fuels* **2002**, *16*, 1463–1469.
- (32) Hicks, J. C.; Drese, J. H.; Fauth, D. J.; Gray, M. L.; Qi, G.; Jones, C. W. Designing Adsorbents for CO<sub>2</sub> Capture from Flue Gas-Hyperbranched Aminosilicas Capable of Capturing CO<sub>2</sub> Reversibly. *J. Am. Chem. Soc.* **2008**, *130*, 2902–2903.
- (33) Didas, S. A.; Kulkarni, A. R.; Sholl, D. S.; Jones, C. W. Role of Amine Structure on Carbon Dioxide Adsorption from Ultradilute Gas Streams such as Ambient Air. *Chem. Sus. Chem.* **2012**, *5*, 2058–2064.
- (34) Zhang, W.; Ma, D.; Liu, X.; Liu, X.; Bao, X. Perfluorotributylamine as a Probe Molecule for Distinguishing Internal and External Acidic Sites in Zeolites by High-Resolution 1H MAS NMR Spectroscopy. *Chem. Commun.* **1999**, *0*, 1091–1092.
- (35) Mafra, L.; Tomaz, C.; Schneider, S.; Wiper, P. V.; Pires, J.; Gomes, J. R. B.; Pinto, M. L. Structure of Chemisorbed CO<sub>2</sub> Species in Amine-Functionalized Mesoporous Silicas Studied by Solid-State NMR and Computer Modeling. *J. Am. Chem. Soc.* **2017**, *139*, 389–408.
- (36) Lee, W. R.; Kim, J. E.; Lee, S. J.; Kang, M.; Kang, D. W.; Lee, H. Y.;

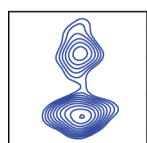
- Hiremath, V.; Seo, J. G.; Jun, H.; Moon, D.; et al. Diamine-Functionalization of a Metal – Organic Framework Adsorbent for Superb Carbon Dioxide Adsorption and Desorption Properties. *Chem. Sus. Chem.* **2018**, *11*, 1694–1707.
- (37) Nandy, A.; Forse, A. C.; Witherspoon, V. J.; Reimer, J. A. NMR Spectroscopy Reveals Adsorbate Binding Sites in the Metal – Organic Framework UiO-66(Zr). *J. Phys. Chem. C* **2018**, *122*, 8295–8305.
- (38) Zhang, Y.; Lucier, B. E. G.; Fischer, M.; Gan, Z.; Boyle, P. D.; Desveaux, B.; Huang, Y. A Multifaceted Study of Methane Adsorption in Metal – Organic Frameworks by Using Three Complementary Techniques. *Chem. Eur. J.* **2018**, *24*, DOI:10.1002/chem.201800424.
- (39) Mason, J. A.; McDonald, T. M.; Bae, T.; Bachman, J. E.; Sumida, K.; Dutton, J. J.; Kaye, S. S.; Long, R. Application of a High-Throughput Analyzer in Evaluating Solid Adsorbents for Post-Combustion Carbon Capture via Multicomponent Adsorption of CO<sub>2</sub>, N<sub>2</sub>, and H<sub>2</sub>O. *J. Am. Chem. Soc.* **2015**, *137*, 4787–4803.
- (40) Flaig, R. W.; Popp, T. M. O.; Fracaroli, A. M.; Kapustin, E. A.; Kalmutzki, M. J.; Altamimi, R. M.; Fathieh, F.; Reimer, J. A.; Yaghi, O. M. The Chemistry of CO<sub>2</sub> Capture in an Amine-Functionalized Metal–Organic Framework under Dry and Humid Conditions. *J. Am. Chem. Soc.* **2017**, *139*, 12125–12128.
- (41) Chen, C.-H.; Shimon, D.; Lee, J. J.; Didas, S. A.; Mehta, A. K.; Sievers, C.; Jones, C. W.; Hayes, S. E. Spectroscopic Characterization of Adsorbed <sup>13</sup>C CO<sub>2</sub> on 3-Aminopropylsilyl-Modified SBA15 Mesoporous Silica. *Environ. Sci. Technol.* **2017**, *51*, 6553–6559.
- (42) Shimon, D.; Chen, C.-H.; Lee, J. J.; Didas, S. A.; Sievers, C.; Jones, C. W.; Hayes, S. E. 15N Solid State NMR Spectroscopic Study of Surface Amine Groups for Carbon Capture: 3-Aminopropylsilyl Grafted to SBA-15 Mesoporous Silica. *Environ. Sci. Technol.* **2018**, *52*, 1488–1495.
- (43) Aresta, M.; Ballivet-Tkatchenko, D.; Dell'Amico, D. B.; Bonnet, M. C.; Boschi, D.; Calderazzo, F.; Faure, R.; Labellac, L.; Marchettie, F. Isolation and Structural Determination of Two Derivatives of the Elusive Carbamic Acid. *Chem Commun.* **2000**, *8*, 1099–1100.
- (44) Pinto, M. L.; Mafra, L.; Guil, J. M.; Pires, J.; Rocha, J. Adsorption and Activation of CO<sub>2</sub> by Amine-Modified Nanoporous Materials Studied by Solid-State NMR and <sup>13</sup>CO<sub>2</sub> Adsorption. *Chem. Mater.* **2011**, *23*, 1387–1395.
- (45) Foo, G. S.; Lee, J. J.; Chen, C.; Hayes, S. E.; Sievers, C.; Jones, C. W. Elucidation of Surface Species through in Situ FTIR Spectroscopy of Carbon Dioxide Adsorption on Amine-Grafted SBA-15. *Chem. Sus. Chem.* **2017**, *10*, 266–276.
- (46) Moore, J. K.; Sakwa-novak, M. A.; Chaikittisilp, W.; Mehta, A. K.; Conradi, M. S.; Jones, C. W.; Hayes, S. E. Characterization of a Mixture of CO<sub>2</sub> Adsorption Products in Hyperbranched Aminosilica Adsorbents by <sup>13</sup>C Solid-State NMR. *Environ. Sci. Technol.* **2015**, *49*, 13684–13691.
- (47) Berglund, B.; Vaughan, R. W. Correlations between Proton Chemical Shift Tensors, Deuterium Quadrupole Couplings, and Bond Distances for Hydrogen Bonds in Solids. *J. Chem. Phys.* **1980**, *73*, 2037–2043.
- (48) Aliev, A. E.; Mann, S. E.; Rahman, A. S.; McMillan, P. F.; Cora, F.; Iuga, D.; Hughes, C. E.; Harris, K. D. M. High-Resolution Solid-State <sup>2</sup>H NMR Spectroscopy of Polymorphs of Glycine. *J. Phys. Chem. A* **2011**, *115*, 12201–12211.
- (49) Stievano, L.; Tielens, F.; Folliet, N.; Gervais, C.; Costa, D. Density Functional Theory Modeling and Calculation of NMR Parameters: An Ab Initio Study of the Polymorphs of Bulk Glycine. *Cryst. Growth Des.* **2010**, *10*, 3657–3667.
- (50) Lee, J. J.; Chen, C.-H.; Shimon, D.; Hayes, S. E.; Sievers, C.; Jones, C. W. Effect of Humidity on the CO<sub>2</sub> Adsorption of Tertiary Amine Grafted SBA-15. *J. Phys. Chem. C* **2017**, *121*, 23480–23487.
- (51) Chen, C.; Shimon, D.; Lee, J. J.; Mentink-vigier, F.; Hung, L.; Sievers, C.; Jones, C. W.; Hayes, S. E. The “Missing” Bicarbonate in CO<sub>2</sub> Chemisorption Reactions on Solid Amine Sorbents. *J. Am. Chem. Soc.* **2018**, DOI:10.1021/jacs.8b04520.
- (52) Čendak, T.; Sequeira, L.; Sardo, M.; Valente, A.; Pinto, M. L.; Mafra, L. Detecting Proton-Transfer in CO<sub>2</sub> Species Chemisorbed on Amine-Modified Mesoporous Silicas Using <sup>13</sup>C NMR Chemical Shift Anisotropy and Smart Control of Amine Surface Density. *Chem. Eur. J.* <https://doi.org/10.1002/chem.201800930>.
- (53) Kieslich, G.; Kumagai, S.; Butler, K. T.; Okamura, T.; Hendon, C. H.; Sun, S.; Yamashita, M.; Walsh, A.; Cheetham, A. K. Role of Entropic Effects in Controlling the Polymorphism in Formate ABX<sub>3</sub> Metal-Organic Frameworks. *Chem Comm.* **2015**, *51*, 15538–15541.
- (54) Xiao, D. J.; Oktawiec, J.; Milner, P. J.; Long, J. R. Pore Environment Effects on Catalytic Cyclohexane Oxidation in Expanded Fe<sub>2</sub>(dobdc) Analogues. *J. Am. Chem. Soc.* **2016**, *138*, 14371–14379.
- (55) Massiot, D.; Fayon, F.; Capron, M.; King, L.; Le Calvé, S.; Alonso, B.; Durand, J.-O.; Bujoli, B.; Gan, Z.; Hoatson, G. Modelling One- and Two-Dimensional Solid-State NMR Spectra. *Magn. Reson. Chem.* **2002**, *40*, 70–76.
- (56) Bertani, P.; Raya, J.; Bechinger, B. 15N Chemical Shift Referencing in Solid State NMR. *Solid State Nucl. Magn. Reson.* **2014**, *61*–62, 15–18.
- (57) Bernard, G. M.; Goyal, A.; Miskolzie, M.; McKay, R.; Wu, Q.; Wasylshen, R. E.; Michaelis, V. K. Methylammonium Lead Chloride: A Sensitive Sample for an Accurate NMR Thermometer. *J. Magn. Reson.* **2017**, *283*, 14–21.
- (58) Blöchl, P. E. Projector Augmented-Wave Method. *Phys. Rev. B* **1994**, *50*, 17953–17979.
- (59) Kresse, G.; Joubert, D. From Ultrasoft Pseudopotentials to the Projector Augmented-Wave Method. *Phys. Rev. B* **1999**, *59*, 1758–1775.
- (60) Kresse, G.; Hafner, J. Ab Initio Molecular Dynamics for Liquid Metals. *Phys. Rev. B* **1993**, *47*, 558–561.
- (61) Kresse, G.; Furthmüller, J. Efficient Iterative Schemes for Ab Initio Total-Energy Calculations Using a Plane-Wave Basis Set. *Phys. Rev. B* **1996**, *54*, 11169–11186.
- (62) Kresse, G.; Furthmüller, J. Efficiency of Ab-Initio Total Energy Calculations for Metals and Semiconductors Using a Plane-Wave Basis Set. *Comput. Mater. Sci.* **1996**, *6*, 15–50.
- (63) Kresse, G.; Hafner, J. Ab Initio Molecular-Dynamics Simulation of the Liquid-Metal–amorphous-Semiconductor Transition in Germanium. *Phys. Rev. B* **1994**, *49*, 14251–14269.
- (64) Lee, K.; Murray, É. D.; Kong, L.; Lundqvist, B. I.; Langreth, D. C. A Higher-Accuracy van Der Waals Density Functional. *Phys. Rev. B* **2010**, *82*, 81101.
- (65) Elsässer, C.; Fahnle, M.; Chan, C. T.; Ho, K. M. Density-Functional Energies and Forces with Gaussian-Broadened Fractional Occupations. *Phys. Rev. B* **1994**, *49*, 13975–13978.
- (66) Perdew, J. P.; Burke, K.; Ernzerhof, M. Generalized Gradient Approximation Made Simple. *Phys. Rev. Lett.* **1996**, *77*, 3865–3868.
- (67) Grimme, S.; Antony, J.; Ehrlich, S.; Krieg, H. A Consistent and Accurate Ab Initio Parametrization of Density Functional Dispersion Correction (DFT-D) for the 94 Elements H-Pu. *J. Chem. Phys.* **2010**, *132*, 154104.
- (68) Grimme, S.; Ehrlich, S.; Goerigk, L. Effect of the Damping Function in Dispersion Corrected Density Functional Theory. *J. Comput. Chem.* **2011**, *32*, 1456–1465.
- (69) Baia, M.; Widdifield, C. M.; Dumez, J.-N.; Thompson, H. P. G.; Cooper, T. G.; Salager, E.; Bassil, S.; Stein, R. S.; Lesage, A.; Day, G. M.; et al. Powder Crystallography of Pharmaceutical Materials by Combined Crystal Structure Prediction and Solid-State <sup>1</sup>H NMR Spectroscopy. *Phys. Chem. Chem. Phys.* **2013**, *15*, 8069–8080.



$\delta^1\text{H}$  (ppm)

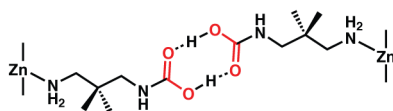


ammonium carbamate chains



$\delta^1\text{H}$  (ppm)

$\delta^{13}\text{C}$  (ppm)



carbamic acid pairs